

INVESTIGATING FEEDBACK AND RELAXATION IN CLUSTERS OF
GALAXIES WITH THE CHANDRA X-RAY OBSERVATORY

By

Kenneth W. Cavagnolo

AN ABSTRACT OF A DISSERTATION

Submitted to
Michigan State University
in partial fulfillment of the requirements
for the degree of

DOCTOR OF PHILOSOPHY

Department of Physics and Astronomy

2008

Dr. Megan Donahue

ABSTRACT

INVESTIGATING FEEDBACK AND RELAXATION IN CLUSTERS OF
GALAXIES WITH THE CHANDRA X-RAY OBSERVATORY

By

Kenneth W. Cavagnolo

INVESTIGATING FEEDBACK AND RELAXATION IN CLUSTERS OF
GALAXIES WITH THE CHANDRA X-RAY OBSERVATORY

By

Kenneth W. Cavagnolo

A DISSERTATION

Submitted to
Michigan State University
in partial fulfillment of the requirements
for the degree of

DOCTOR OF PHILOSOPHY

Department of Physics and Astronomy

2008

ABSTRACT

INVESTIGATING FEEDBACK AND RELAXATION IN CLUSTERS OF
GALAXIES WITH THE CHANDRA X-RAY OBSERVATORY

By

Kenneth W. Cavagnolo

Copyright by
KENNETH W. CAVAGNOLO
2008

Dedicated to my mother: Miss Lorna Lorraine Cox.

ACKNOWLEDGMENTS

Thanks to Christopher Waters for the L^AT_EX class used to format this thesis.

My deepest thanks to Megan Donahue and Mark Voit for their guidance, wisdom, patience, and without whom I would be in quantum computing. I can only say, “Thank you, Megan” for giving me the time and space to find my bearings after my mother’s passing, words are insufficient to express my gratitude. Ming Sun always listened, always had time for a question, and was never wrong. Jack Baldwin nurtured my painfully slow development as a research assistant, a more calming voice there has never been. On behalf of everyone that has never said so, “We love you, Shawna Prater. MSU Astronomy and Astrophysics cannot do business without you.” And of course, Debbie Simmons, without whom I would have been dropped from all courses and locked out of the building.

Many dissertations across many disciplines acknowledge many religious figures and a multitude of gods; but what about the Sun? Every time I feel the startling warmth of the Sun on my skin, it is an invigorating experience. To be bathed in photons millions of years old from an inconceivably large nuclear power plant over a hundred million kilometers away makes me feel connected to the Universe in a way that is surreal. To feel purposely cared for by an absentee whom’s existence and operation are fundamentally devoid of purpose is quite profound. Unknowingly, the Sun gave rise to a species of sentient dissidents. For that I say, “Thank you, Sun!”

To my wife: Our vows were fortelling, I will indeed require the course of an entire life to express my appreciation for the tenderness, care, love, and humor you gave during completion of this dissertation. You are, and always will be, my beloved.

PREFACE

Our Universe is predominantly an untold story. Within a larger, nested framework of complex mechanisms, humans evolved with minimal impact on the systems which support and nurture our existence. Yet, during the short era of global industrialization, we have compromised the effectiveness and function of the systems which formed the biodiversity which makes our planet such a wonderful place. As an acknowledgement of the appreciation our species has for the Earth, and as a show of our understanding for humanity's fleeting presence in the Earth's lifecycle, let us strive to utilize the pursuit of knowledge, through application of reason and logic, so that our actions benefit "all the children, of all species, for all of time" (McDonough & Braungart, 2002). Let us all exert effort such that the Earth and the Universe will be enriched by humanity, and that our actions – local, global, and possibly interplanetary – will leave the places we inhabit and visit nourished from our presence.

TABLE OF CONTENTS

List of Tables	vii
List of Figures	viii
List of Symbols	ix
1 Introduction	1
1.1 Clusters of Galaxies	1
1.2 The Incomplete Picture of Clusters	6
1.2.1 Breaking of Self-Similarity	7
1.2.2 The Cooling Flow Problem	11
1.3 The Intracluster Medium	16
1.3.1 X-ray Emission	17
1.3.2 Entropy	23
1.4 Chandra X-Ray Observatory	26
1.4.1 Telescope and Instruments	26
1.4.2 Calibration, Background, and Lifetime	30
2 Bandpass Dependence of X-ray Temperatures in Galaxy Clusters .	38
3 Chandra Archival Sample of Intracluster Entropy Profiles	40
4 An Entropy Threshold for Strong Hα and Radio Emission in the Cores of Galaxy Clusters	42
5 Summary	43
References	45
A Co-authored Publications	53

LIST OF TABLES

LIST OF FIGURES

1.1	<i>Hubble</i> image of Abell 1689	2
1.2	Composite image of the Bullet Cluster	4
1.3	Figures illustrating of large scale structure formation.	8
1.4	Synthetic spectral model of $kT_X = 2.0$ keV gas.	20
1.5	Synthetic spectral model of $kT_X = 8.0$ keV gas.	20
1.6	<i>Chandra</i> X-ray Observatory spacecraft.	27
1.7	Pre-launch photo of the ACIS instrument	29
1.8	ACIS focal plane during observation.	31
1.9	Spectrum of Abell 1795.	32
1.10	<i>Chandra</i> effective area as a function of energy.	34

Images in this dissertation are presented in color.

LIST OF SYMBOLS

Mpc	Megaparsec: A unit of length representing one million parsecs. The parsec (pc) is a historical unit for measuring parallax and equals 30.857×10^{12} km.	1
z	Dimensionless redshift: As is common in most of astronomy, I adopt the definition of redshift using a dimensionless ratio of wavelengths, $z = (\lambda_{\text{observed}}/\lambda_{\text{rest}}) - 1$, where the wavelength shift occurs because of cosmic expansion.	1
H_0	Hubble constant: The current ratio of recessional velocity arising from expansion of the Universe to an object's distance from the observer, $v = H_0 D$. H_0 is currently measured to be $\sim 70 \text{ km s}^{-1} \text{ Mpc}^{-1}$. Inverted, the Hubble constant yields the present age of the Universe, $H_0^{-1} \approx 13.7$ billion years. $H(z)$ denotes the Hubble constant at a particular redshift, z	1
ρ_c	Critical density: The density necessary for a universe which has spatially flat geometry and in which the expansion rate of spacetime balances gravitational attraction and prevents recollapse. In terms of relevant quantities $\rho_c = 3H(z)^2/8\pi G$, with units g cm^{-3}	1
Ω_Λ	Cosmological constant energy density of the Universe: The ratio of energy density due to a cosmological constant to the critical density. Ω_Λ is currently measured to be ~ 0.7	1
Ω_M	Matter density of the Universe: The ratio of total matter density to the critical density. Ω_M is currently measured to be ~ 0.3	1
M_\odot	Mass of the Sun: One solar mass equals $1.9891 \times 10^{30} \text{ kg}$	3
D_C	Comoving distance: The distance which would be measured between two objects today if those two points were moving away from each other with the expansion of the Universe.	9
D_A	Angular diameter distance: The ratio of an object's true transverse size to its angular size. For a nearly flat universe, D_A is a good approximation of the comoving distance, $D_A \approx D_C/(1+z)$	9
Ω_S	Solid angle: For a sphere of a given radius, for example the distance to an object D_C , the area of that object, A , on the sphere subtends an angle equal to $\Omega_S = A/D_C^2$. This is the solid angle.	9
V_C	Comoving volume: The volume in which the number density of slowly evolving objects locked into the local Hubble flow, like galaxy clusters, is constant with redshift. For a redshift elements dz and solid angle $d\Omega_S$ the comoving volume element is $dV_C = \frac{D_C[D_A(1+z)]^2}{\sqrt{\Omega_M(1+z)^3 + \Omega_k(1+z)^2 + \Omega_\Lambda}} d\Omega_S dz$ where Ω_k is curvature and is ≈ 0	9
Z_\odot	Metal abundance of the Sun: Individual elemental abundances can be found in ?.	19

N_H	Neutral hydrogen column density: The Galaxy is rich with neutral hydrogen which absorbs incoming extragalactic radiation. Photoelectric absorption models are used to quantify the attenuation, and typically take as input the column density (cm^{-2}) of neutral hydrogen in a particular direction. N_H is related to the number density, n_H (cm^{-3}), along the line of sight, dl , as $N_H = \int n_H dl$	20
Λ	Cooling function: A function describing plasma emissivity for a given temperature and metal composition, and typically given in units of $\text{ergs cm}^3 \text{s}^{-1}$	22

CHAPTER 1:

INTRODUCTION

1.1 CLUSTERS OF GALAXIES

Of the luminous matter in the Universe, stars and galaxies are often the most familiar to a sky gazer. Aside from the Moon and the occasional bright planet, stars are the most abundantly obvious patrons of the night sky. Viewed from a sufficiently dark location, the stars form a band of light interspersed with dust and gaseous clouds which define the Milky Way, our home galaxy. The Milky Way is only one of more than 30 galaxies in a gravitationally bound group of galaxies, named the Local Group, which includes the well-known, nearby galaxy Andromeda. But in cosmological terms, the Local Group is very small in comparison to immense structures containing thousands of galaxies. In a turn of wit, these structures are appropriately named clusters of galaxies, and are the focus of this dissertation.

Galaxy clusters are the most massive gravitationally bound structures to have yet formed in the Universe. As where galaxy groups have roughly 10-50 galaxies, galaxy clusters have hundreds to thousands of galaxies. When viewed through a telescope, a galaxy cluster appears as a tight distribution of mostly elliptical and S0 spiral galaxies within a radius of $\sim 1 - 5 \text{ Mpc}^1$ of each other. Rich galaxy clusters are truly spectacular objects, as can be seen in Figure 1.1 which shows the *Hubble* Space Telescope's close-up of the strong lensing cluster Abell 1689.

¹Throughout this dissertation, a flat Λ CDM cosmology of $H_0 = 70 \text{ km s}^{-1} \text{ Mpc}^{-1}$, $\Omega_\Lambda = 0.7$, and $\Omega_M = 0.3$ is assumed. These values are taken from Spergel et al. (2007).

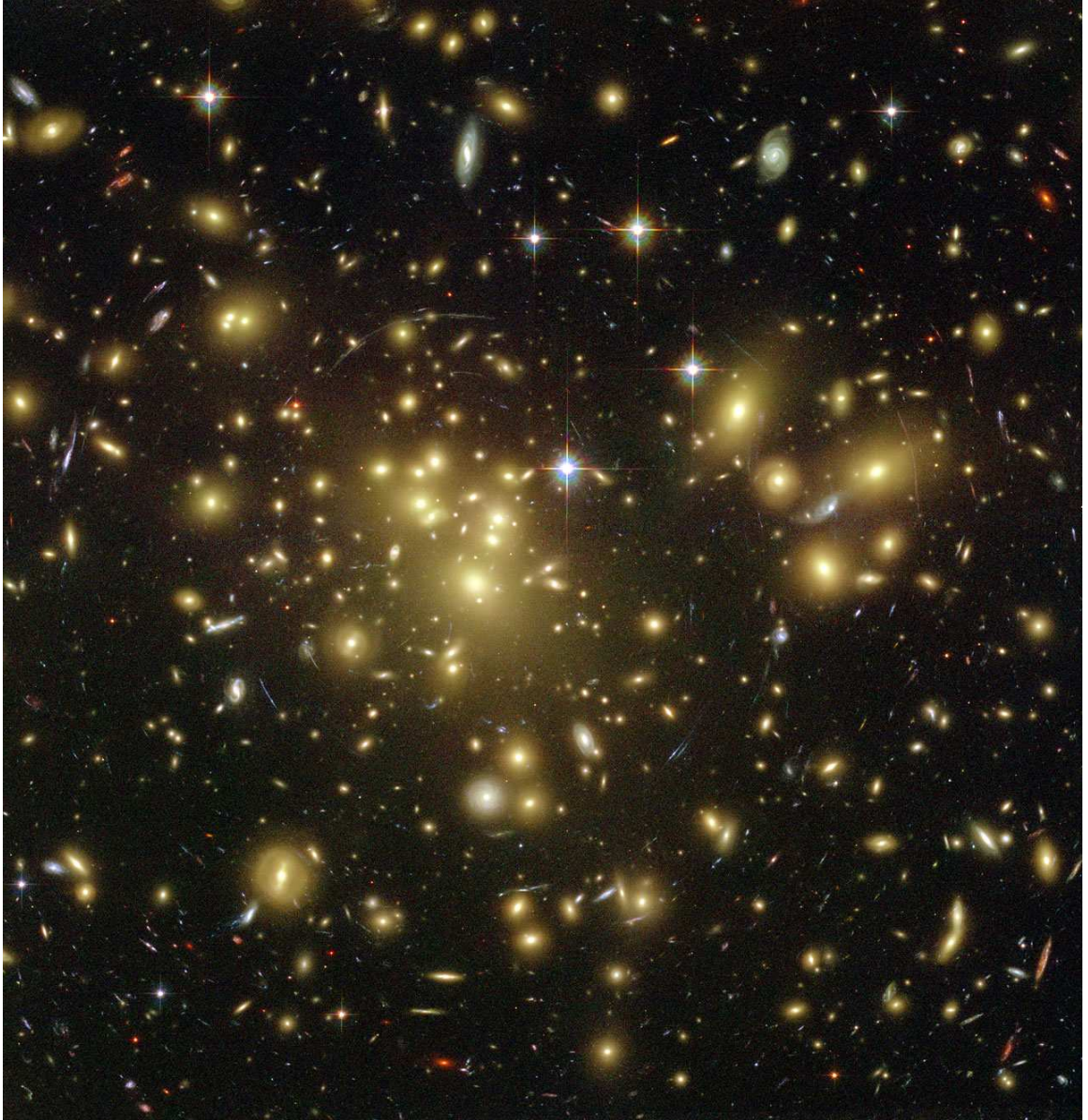


Figure 1.1 Optical image of the galaxy cluster Abell 1689 as observed with the ACS instrument on-board the *Hubble* Space Telescope. The fuzzy yellowish spheres are giant elliptical (gE) galaxies in the cluster, with the gE nearest the center of the image being the brightest cluster galaxy – ostensibly, the cluster “center”. Image taken from NASA’s Hubblesite.org. Image Credits: NASA, N. Benitez (JHU), T. Broadhurst (The Hebrew University), H. Ford (JHU), M. Clampin(STScI), G. Hartig (STScI), G. Illingworth (UCO/Lick Observatory), the ACS Science Team and ESA.

Galaxy clusters are deceptively named. As with most objects in the Universe, one of the most revealing characteristics of an object is its mass, and the mass of clusters of galaxies are not dominated by galaxies. With the proper vision, an observer would find clusters are dominated ($\gtrsim 70\%$) by dark matter with most ($\gtrsim 80\%$) of the baryonic mass² in the form of a hot ($kT \approx 2 - 15$ keV; 10-100 million degrees K), luminous (10^{43-46} ergs s⁻¹), diffuse ($10^{-1} - 10^{-4}$ cm⁻³) intracluster medium (ICM) which is co-spatial with the galaxies but dwarfs them in mass (Blumenthal et al., 1984; David et al., 1990). For comparison, the ICM in the core region of a galaxy cluster is, on average, 10^{20} times less dense than typical Earth air, 10^5 times denser than the mean cosmic density, more than 2000 times hotter than the surface of the Sun, and shines as bright as 10^{35} 100 watt light bulbs.

Because of the ICM's extreme temperature, the gas is mostly ionized, making it a plasma. For the temperature range of clusters, the ICM is most luminous at X-ray wavelengths of the electromagnetic spectrum. This makes observing galaxy clusters with X-ray telescopes, like NASA's *Chandra* X-ray Observatory, a natural choice. Clusters have masses ranging over $10^{14-15} M_{\odot}$ with velocity dispersions of $500 - 1500$ km s⁻¹. The ICM has also been enriched with metals³ to an average value of ~ 0.3 solar abundance. Shown in Figure 1.2 is an optical, X-ray, and gravitational lensing composite image of the galaxy cluster 1E0657-56. This cluster is undergoing an especially spectacular and rare merger in the plane of the sky which allows for the separate dominant components of a cluster – dark matter, the ICM, and galaxies – to be “seen” distinctly.

Knowing the characteristics of galaxy clusters is a small part of the discovery process, we must also wonder, why study clusters of galaxies? Galaxy clusters have two very important roles in the current research paradigm:

²Baryonic is a convenient term used to describe ordinary matter like atoms or molecules, while non-baryonic matter is more exotic like free electrons or dark matter particles.

³It is common practice in astronomy to classify “metals” as any element with more than two protons.

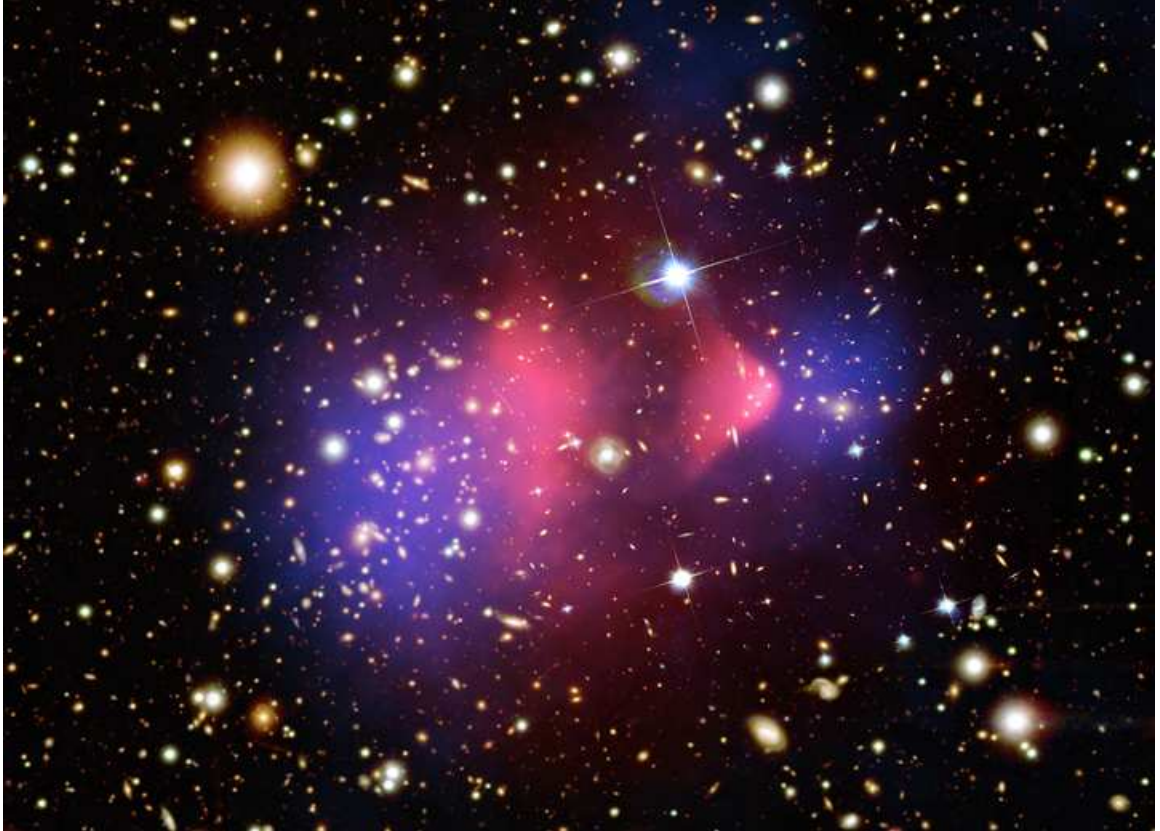


Figure 1.2 The galaxy cluster 1E0657-56, a.k.a. the Bullet Cluster. All of the primary components of a galaxy cluster can be seen in this image: the X-ray ICM (pink), dark matter (blue), and galaxies. The brilliant white object with diffraction spikes is a star. This cluster has become very famous because it is direct evidence for the existence of dark matter (Clowe et al., 2006). Image taken from NASA Press Release 06-297. Image credits: NASA/CXC/CfA/Markevitch et al. (2002) (X-ray); NASA/STScI/Magellan/U.Arizona/Clowe et al. (2006) (Optical); NASA/STScI/ESO WFI/Magellan/U.Arizona/Clowe et al. (2006) (Lensing).

1. Galaxy clusters represent a unique source of information about the Universe’s underlying cosmological parameters, including the nature of dark matter and the dark energy equation of state. Large-scale structure growth is exponentially sensitive to some of these parameters, and by counting the number of clusters found in a comoving volume of space, specifically above a given mass threshold, clusters may be very useful in cosmological studies (Voit, 2005).
2. The cluster gravitational potential well is deep enough to retain all the matter which has fallen in over the age of the Universe. This slowly evolving “sealed box” therefore contains a comprehensive history of all the physical processes involved in galaxy formation and evolution, such as: stellar evolution, supernovae feedback, black hole activity in the form of active galactic nuclei, galaxy mergers, ram pressure stripping of in-falling galaxies and groups, *et cetera*. The time required for the ICM in the outskirts of a cluster to radiate away its thermal energy is longer than the age of the Universe, hence the ICM acts as a record-keeper of all the aforementioned activity. Therefore, by studying the ICM’s physical properties, the thermal history of the cluster can be partially recovered and utilized in developing a better understanding of cluster formation and evolution.

In this dissertation I touch upon both these points by studying the emergent X-ray emission of the ICM as observed with the *Chandra* X-ray Observatory.

While clusters have their specific uses in particular areas of astrophysics research, they also are interesting objects in their own right. A rich suite of physics are brought to bear when studying galaxy clusters. A full-blown, theoretical construction of a galaxy cluster requires, to name just a few: gravitation, fluid mechanics, thermodynamics, hydrodynamics, magnetohydrodynamics, and high-energy/particle/nuclear physics. Multiwavelength observations of galaxy clusters provide excellent datasets for testing the theoretical predictions from other areas of physics, and clusters are

also a unique laboratory for empirically establishing how different areas of physics interconnect. Just this aspect of clusters puts them in a special place among the objects in our Universe worth intense, time-consuming, (and sometimes expensive) scrutiny. At a minimum, galaxy clusters are most definitely worthy of being the focus of a humble dissertation from a fledgling astrophysicist.

In Section §1.2, I more thoroughly discuss reasons for studying clusters of galaxies which are specific to this dissertation. Presented in Section §1.2.1 is discussion of why clusters of different masses are not simply scaled versions of one another, and in Section §1.2.2 the unresolved “cooling flow problem” is briefly summarized. As this is a dissertation focused around observational work, in Section §1.3 I provide a brief primer on the X-ray observable properties of clusters which are important to understanding this dissertation. Section §1.3.2 provides discussion of gas entropy, a physical property of the ICM which may be unfamiliar to many readers and is utilized heavily in Chapters ?? and 4. The chapter concludes with a brief description of the *Chandra* X-ray Observatory (CXO) and its instruments in Section §1.4. *Chandra* is the space-based telescope with which all of the data presented in this dissertation was collected.

1.2 THE INCOMPLETE PICTURE OF CLUSTERS

The literature on galaxy clusters is extensive. There has been a great deal already written about clusters (with much more eloquence), and I strongly suggest reading Mushotzky (1984); Kaiser (1986); Evrard (1990); Kaiser (1991); Sarazin (1986); Fabian (1994); Voit (2005); Peterson & Fabian (2006); Markevitch & Vikhlinin (2007); McNamara & Nulsen (2007) (and references therein) for a comprehensive review of the concepts and topics to be covered in this dissertation. The discussion of Sections §1.2.1 and §1.2.2 focuses on a few unresolved mysteries involving galaxy clusters: the cooling flow problem as it relates to galaxy formation and the breaking of self-

similarity in relation to using clusters in cosmological studies.

1.2.1 BREAKING OF SELF-SIMILARITY

We now know the evolution of, and structure within, the Universe are a direct result of the influence from dark energy and dark matter. An all pervading repulsive dark energy has been posited to be responsible for the accelerating expansion of the Universe (Riess et al., 1998; Perlmutter et al., 1999; Riess et al., 2007). Dark matter is an unknown form of matter which interacts with itself and ordinary matter (both baryonic and non-baryonic) through gravitational forces. Up until the last ~ 5 billion years (Riess et al., 1998; Perlmutter et al., 1999; Riess et al., 2007), the influence of dark matter on the Universe has been greater than that of dark energy. The early dominance of dark matter is evident from the existence of large-scale structure like galaxy clusters.

An end result of the gravitational attraction between amalgamations of dark matter particles, called dark matter halos, is the merger of small halos into ever larger halos. Since dark matter far outweighs baryonic matter in the Universe, the baryons are coupled to the dark matter halos via gravity, and hence are dragged along during the halo merger process. Like raindrops falling in a pond that drains into a river which flows into the ocean, the process of smaller units merging to create larger units is found *ad infinitum* in the Universe and is given the name hierarchical structure formation. A useful visualization of the hierarchical structure formation process is shown in Fig. 1.3. Hierarchical formation begins with small objects like the first stars, continues on to galaxies, and culminates in the largest present objects, clusters of galaxies.

In a very simplistic redux, dark energy is attempting to push space apart while dark matter is attempting to pull matter together within that space. Were the balance and evolution of dark energy and dark matter weighted heavily toward one or the other

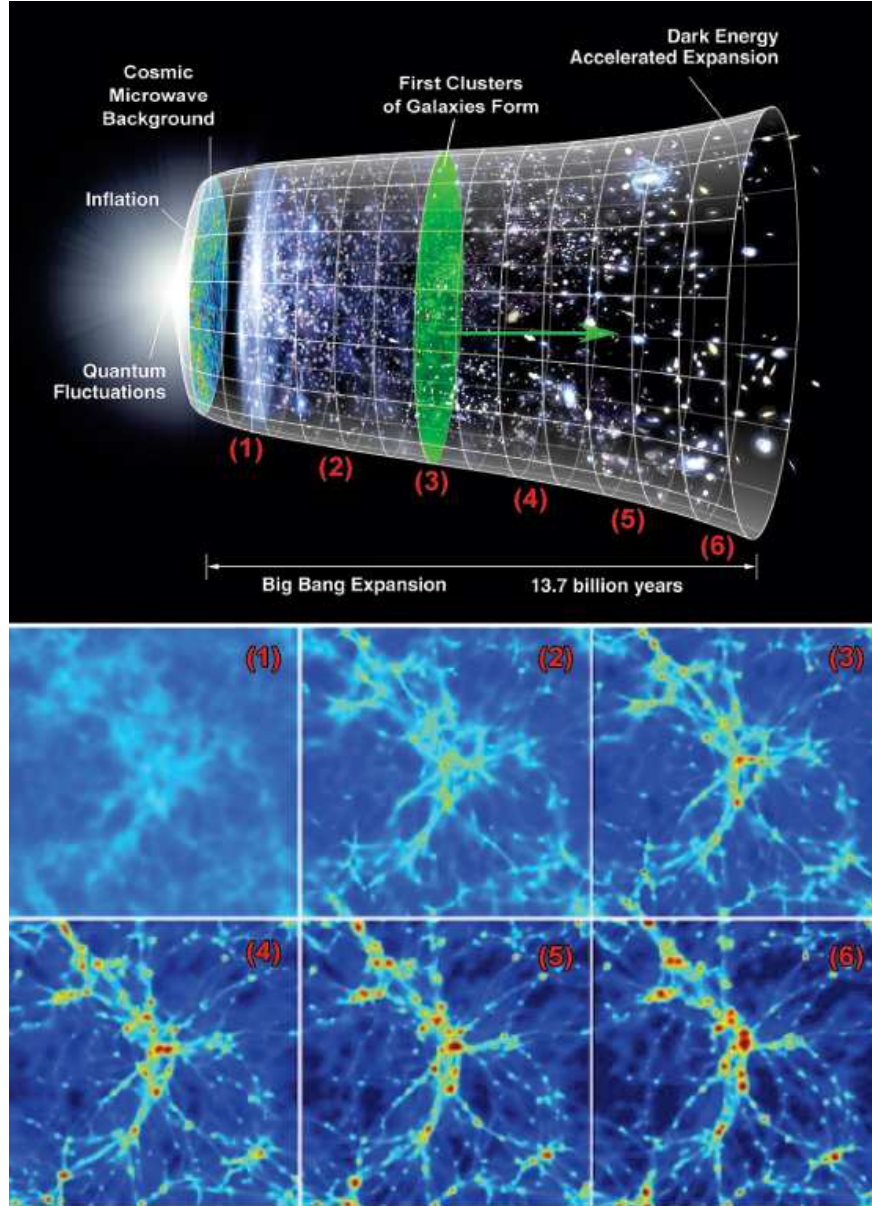


Figure 1.3 *Top panel:* Illustration of hierarchical structure formation. *Bottom panel:* Snapshots from the simulation of a galaxy cluster forming. Each pane is 10 Mpc on a side. Color coding represents gas density along the line of sight (deep red is highest, dark blue is lowest). Each snapshot is numbered on the illustration at the approximate epoch each stage of cluster collapse occurs. Notice that, at first (1-2), very small objects like the first stars and proto-galaxies collapse and then these smaller objects slowly merge into much larger halos (3-5). The hierarchical merging process ultimately results in a massive galaxy cluster (6) which continue to grow as sub-clusters near the box edge creep toward the cluster main body. Illustration taken from NASA/WMAP Science Team and modified by author. Simulation snapshots taken from images distributed to the public by the Virgo Consortium on behalf of Dr. Craig Booth: <http://www.virgo.dur.ac.uk>

it becomes clear that the amount of structure and its distribution will be different. Thus, the nature of dark matter and dark energy ultimately influence the number of clusters found at any given redshift (*e.g.* White et al., 1993) and hence cluster number counts are immensely powerful in determining cosmological parameters (*e.g.* Borgani et al., 2001)).

Individual clusters do not yield the information necessary to study the underlying cosmogony. However, the number density of clusters above a given mass threshold within a comoving volume element, (*e.g.* the cluster mass function) is a useful quantity (Voit, 2005). But the cluster mass function is a powerful cosmological tool only if cluster masses can be accurately measured. With no direct method of measuring cluster mass, easily observable properties of clusters must be used as proxies to infer mass.

Reliable mass proxies, such as cluster temperature and luminosity, arise naturally from the theory that clusters are scaled versions of each other. This property is commonly referred to as self-similarity of mass-observables. More precisely, self-similarity presumes that when cluster-scale gravitational potential wells are scaled by the cluster-specific virial radius, the full cluster population has potential wells which are simply scaled versions of one another (Navarro et al., 1995, 1997). Self-similarity is also expected to yield low-scatter scaling relations between cluster properties such as luminosity and temperature (Kaiser, 1986, 1991; Evrard & Henry, 1991; Navarro et al., 1995, 1997; Eke et al., 1998; Frenk et al., 1999). Consequently, mass-observable relations, such as mass-temperature and mass-luminosity, derive from the fact that most clusters are virialized, meaning the cluster’s energy is shared such that the virial theorem, $-2\langle T \rangle = \langle V \rangle$ where $\langle T \rangle$ is average kinetic energy and $\langle V \rangle$ is average potential energy, is a valid approximation. Both theoretical (Evrard et al., 1996; Bryan & Norman, 1998; Mohr et al., 1999; Bialek et al., 2001; Borgani et al., 2002) and observational (Mushotzky, 1984; Edge & Stewart, 1991; White et al., 1997; Allen &

Fabian, 1998a; Markevitch et al., 1998; Arnaud & Evrard, 1999; Finoguenov et al., 2001) studies have shown cluster mass correlates well with X-ray temperature and luminosity, but that there is much larger ($\approx 20 - 30\%$) scatter and different slopes for these relations than expected. The breaking of self-similarity is attributed to non-gravitational processes such as ongoing mergers (Randall et al., 2002), heating via feedback (Cavaliere et al., 1999; Bower et al., 2001), or radiative cooling in the cluster core (Voit & Bryan, 2001; Voit et al., 2002).

To reduce the scatter in mass scaling-relations and to increase their utility for weighing clusters, how secondary processes alter temperature and luminosity must first be quantified. It was predicted that clusters with a high degree of spatial uniformity and symmetry (*e.g.* clusters with the least substructure in their dark matter and gas distributions) would be the most relaxed and have the smallest deviations from mean mass-observable relations. The utility of substructure in quantifying relaxation is prevalent in many natural systems, such as a placid lake or spherical gas cloud of uniform density and temperature. Structural analysis of cluster simulations, take for example the recent work of Jeltima et al. (2007) or Ventimiglia et al. (2008), have shown measures of substructure correlate well with cluster dynamical state. But spatial analysis is at the mercy of perspective. If equally robust aspect-independent measures of dynamical state could be found, then quantifying deviation from mean mass-scaling relations would be improved and the uncertainty of inferred cluster masses could be further reduced. Scatter reduction ultimately would lead to a more accurate cluster mass function, and by extension the constraints on theories explaining dark matter and dark energy could grow tighter.

In Chapter 2, I present work investigating ICM temperature inhomogeneity, which has been proposed as a method for better understanding the dynamical state of a cluster (Mathiesen & Evrard, 2001). Temperature inhomogeneity has the advantage of being a spectroscopic quantity and therefore falls into the class of aspect-independent

metrics which may be useful for reducing scatter in mass-observable relations. In a much larger context, this dissertation may contribute to the improvement of our understanding of the Universe’s make-up and evolution.



1.2.2 THE COOLING FLOW PROBLEM

For 50% – 66% of galaxy clusters, the densest and coolest ($kT_X \lesssim T_{\text{virial}}/2$) ICM gas is found in the central $\sim 10\%$ of the cluster gravitational potential well (Stewart et al., 1984; Edge et al., 1992; White et al., 1997; Peres et al., 1998; Bauer et al., 2005). For the temperature regime of the ICM, radiative cooling time, t_{cool} (see eqn. 1.11), is more strongly dependent on density than temperature, $t_{\text{cool}} \propto T_g^{1/2} \rho^2$, where T_g is gas temperature and ρ is gas density. The energy lost via radiative cooling is seen as diffuse thermal X-ray emission from the ICM (Gursky et al., 1971; Mitchell et al., 1976; Serlemitsos et al., 1977). When thermal energy is radiated away from the ICM, the gas density must increase while gas temperature and internal pressure respond by decreasing. The cluster core gas densities ultimately reached through the cooling process are large enough such that the cooling time required for the gas to radiate away its thermal energy is much shorter than both the age of the Universe, *e.g.* $t_{\text{cool}} \ll H_0^{-1}$, and the age of the cluster (Cowie & Binney, 1977; Fabian & Nulsen, 1977). Without compensatory heating, it thus follows that the ICM in some cluster cores should cool and condense.

Gas within the cooling radius, r_{cool} , (defined as the radius at which $t_{\text{cool}} = H_0^{-1}$) is underpressured and cannot provide sufficient pressure support to prevent overlying gas layers from forming a subsonic flow of gas toward the bottom of the cluster gravitational potential. However, if when the flowing gas enters the central galaxy it has cooled to the point where the gas temperature equals the central galaxy virial temperature, then adiabatic compression⁴ from the galaxy’s gravitational potential well

⁴As the name indicates, no heat is exchanged during adiabatic compression; but gas temperature rises because the internal gas energy increases due to external work being done on the system.

can balance heat losses from radiative cooling. But, if the central galaxy’s gravitational potential is flat, then the gas energy gained via gravitational effects can also be radiated away and catastrophic cooling can proceed.

The sequence of events described above was given the name “cooling flow” (Fabian & Nulsen, 1977; Cowie & Binney, 1977; Mathews & Bregman, 1978) and is the most simplistic explanation of what happens to the ICM when it is continuously cooling, spherically symmetric, and homogeneous (see Fabian, 1994; Peterson & Fabian, 2006; Donahue & Voit, 2004, for reviews). The theoretical existence of cooling flows comes directly from X-ray observations, yet the strongest observational evidence for the existence of cooling flows will be seen when the gas cools below X-ray emitting temperatures and forms stars, molecular clouds, and emission line nebulae. Unfortunately, cooling flow models were first presented at a time when no direct, complementary observational evidence for cooling flows existed, highlighting the Catch-22  or confronting the models. Undeterred, many in the X-ray astrophysics community dubbed all clusters which meet the criterion $t_{\text{cool}} < H_0^{-1}$ “cooling flow clusters,” a tragic twist of nomenclature fate which has plagued many scientific talks. 

A mass deposition rate, \dot{M} , can be inferred for cooling flows based on X-ray observations: $\dot{M} \propto L_X(r < r_{\text{cool}})(kT_X)^{-1}$, where $L_X(r < r_{\text{cool}})$ is the X-ray luminosity within the cooling region, kT_X is the X-ray gas temperature, and \dot{M} typically has units of $M_\odot \text{ yr}^{-1}$. The quantity \dot{M} is useful in getting a handle on how much gas mass is expected to be flowing into a cluster core. Mass deposition rates have been estimated for many clusters and found to be in the range $100\text{--}1000 M_\odot \text{ yr}^{-1}$ (Fabian et al., 1984; White et al., 1997; Peres et al., 1998). Mass deposition rates can also be estimated using emission from individual emission lines: $\dot{M} \propto L_X(r < r_{\text{cool}})\epsilon_f(T)$, where $L_X(r < r_{\text{cool}})$ is the X-ray luminosity within the cooling region and $\epsilon_f(T)$ is the emissivity fraction attributable to a particular emission line. The ICM soft X-ray emission lines, for example of Fe XVII, O VIII, and Ne X at $E < 1.5 \text{ keV}$, are

especially useful in evaluating the properties of cooling flows. Early low-resolution spectroscopy found mass deposition rates consistent with those from X-ray observations (*e.g.* Canizares et al., 1982).

Not surprisingly, the largest, brightest, and most massive galaxy in a cluster, the brightest cluster galaxy (BCG), typically resides at the bottom of the cluster potential, right at the center of where a cooling flow would terminate. Real cooling flows ~~are~~ not expected to be symmetric, laminar, continuous, or in thermodynamic equilibrium with the ambient medium. Under these conditions, thermal instabilities are expected to rapidly develop and collapse to form gaseous molecular clouds and stars. The stellar and gaseous components of ~~BCGs~~ clearly indicate some amount of cooling and mass deposition has occurred. But are the properties of the BCG population consistent with cooling flow model predictions? For example, BCGs should be supremely luminous and continually replenished with young, blue stellar populations since the epoch of their formation. One should then expect the cores of clusters suspected of hosting a cooling flow to have very bright, blue BCGs bathed in clouds of emission line nebulae. However, observations of cooling flow clusters reveal the true nature of the core to ~~be quite to the contrary~~.


The optical properties of BCGs have been known for quite a long time and these massive galaxies are neither as blue or bright as would be expected from the extended periods of growth via cooling flows. While attempts were made in the past to selectively channel the unobserved cool gas into optically dark objects, such as in low-mass, distributed star formation, methodical searches in the optical, infrared, UV, radio, and soft X-ray wavelengths ($kT_X \lesssim 2.0$ keV) have revealed that the total mass of ~~gas~~ associated with cooling flows is much less than expected (Hu et al., 1985; Heckman et al., 1989; McNamara et al., 1990; O’Dea et al., 1994b,a; Antonucci & Barvainis, 1994; McNamara & Jaffe, 1994; Voit & Donahue, 1995; Jaffe & Bremer, 1997; Falcke et al., 1998; Donahue et al., 2000; Edge & Frayer, 2003).

Confirming the suspicion that cooling flows are not cooling as advertised, high-resolution *XMM-Newton* RGS X-ray spectroscopy of clusters expected to host very massive cooling flows definitively proved that the ICM was not cooling to temperatures less than $1/3$ of the cluster virial temperature (Peterson et al., 2001; Tamura et al., 2001; Peterson et al., 2003). A cooling X-ray medium which has emission discontinuities at soft energies is not a feature of the simplest single-phase cooling flow models, and a troubling amount of fine-tuning must be added to agree with observations. Modifications such as preferential absorption of soft X-rays in the core region (*e.g.* Allen et al., 1993) or turbulent mixing of a multi-phase cooling flow (*e.g.* Fabian et al., 2002) have been successful in matching observations, but these models lack the universality needed to explain why *all* cooling flows are not as massive as expected.

All of the observational evidence has resulted in a two-component “cooling flow problem”: (1) spectroscopy of soft X-ray emission from cooling flow clusters is inconsistent with theoretical predictions, and (2) multiwavelength observations reveal a lack of cooled gas mass or stars to account for the enormous theoretical mass deposition rates implied by simple cooling flow models. So why and how is the cooling of gas below $T_{\text{virial}}/3$ suppressed? As is the case with most questions, the best answer thus far is simple: the cooling flow rates were wrong, with many researchers suggesting the ICM has been **intermitently** heated. But what feedback mechanisms are responsible for hindering cooling in cluster cores? How do these mechanisms operate? What observational constraints can we find to determine which combination of feedback mechanism hypotheses are correct? The answers to these questions have implications for both cluster evolution and massive galaxy formation.

The cores of clusters are active places, so finding heating mechanisms is not too difficult. The prime suspect, and best proposed solution to the cooling flow problem thus far, invokes some combination of supernovae and outbursts from the active galactic nucleus (AGN) in the BCG (Binney & Tabor, 1995; Bower, 1997; Loewenstein,

2000; Voit & Bryan, 2001; Churazov et al., 2002; Brüggen & Kaiser, 2002; Brüggen et al., 2002; Nath & Roychowdhury, 2002; Ruszkowski & Begelman, 2002; Alexander, 2002; Omma et al., 2004; McCarthy et al., 2004; Roychowdhury et al., 2004; Hoeft & Brüggen, 2004; Dalla Vecchia et al., 2004; Soker & Pizzolato, 2005; Pizzolato & Soker, 2005; Voit & Donahue, 2005; Brighenti & Mathews, 2006; Mathews et al., 2006). However, there is a serious scale mismatch in heating and cooling processes which has hampered the development of a self-regulating feedback loop involving AGN. Radiative cooling proceeds as the square of gas density, whereas heating is proportional to volume. Hence, modeling feedback with a small source object, $r \sim 1$ pc, that is capable of compensating for radiative cooling losses over an $\approx 10^6$ kpc³ volume, where the radial density can change by four orders of magnitude, is quite difficult. A

 **very wise person** once framed this problem as, “trying to heat the whole of Europe with something the size of a button.”

The basic model of how AGN feedback works is that first gas accretes onto a supermassive black hole at the center of the BCG, resulting in the acceleration and ejection of very high energy particles back into the cluster environment. The energy released in an AGN outburst is of order 10^{58-61} ergs. Under the right conditions, and via poorly understood mechanisms, energy output by the AGN is transferred to the ICM and thermalized, thereby heating the gas. The details of how this process operates is beyond the scope of this dissertation (see McNamara & Nulsen, 2007, for a recent review). However, in this dissertation I do investigate some observable properties of clusters which are directly impacted by feedback mechanisms.

Utilizing the quantity ICM entropy, I present results in Chapter ?? which show that radial ICM entropy distributions for a large sample of clusters have been altered in ways which are consistent with AGN feedback models. Entropy and its connection to AGN feedback is discussed in Subsection 1.3.2 of this Introduction. In Chapter 4 I also present observational results which support the hypothesis of Voit et al. (2008)

that electron thermal conduction may be an important mechanism in distributing AGN feedback energy. Hence, this dissertation, in small part, seeks to add to the understanding of how feedback functions in clusters, and thus how to resolve the cooling flow problem. The resolution of which will lead to better models of galaxy formation and cluster evolution.

1.3 THE INTRACLUSTER MEDIUM


In the Introduction, the ICM was presented as a mostly ionized, hot, diffuse plasma which dominates the baryonic mass content of clusters. But where did it come from and what is the composition of this pervasive ICM? What are the mechanisms that result in the ICM's X-ray luminescence? How do observations of the ICM get converted into physical properties of a cluster? In this section I briefly cover the answers to these questions in order to give the reader a better understanding of the ICM.

Galaxy clusters are built-up during the process of hierarchical merger of dark matter halos and the baryons gravitationally coupled to those halos (White & Rees, 1978). Owing to the inefficiency of galaxy formation and the processes of galactic mass ejection and ram pressure stripping, many of the baryons in these dark matter halos are in the form of diffuse gas and not locked up in galaxies. During the merger of dark matter halos, gravitational potential energy is converted to thermal energy and the diffuse gas is heated to the virial temperature of the cluster potential through processes like adiabatic compression and accretion shocks. The cluster virial temperature is calculated by equating the average kinetic energy of a gas particle to its thermal energy,

$$\frac{1}{2}\mu m\langle\sigma^2\rangle = \frac{3}{2}kT_{\text{virial}} \quad (1.1)$$

$$T_{\text{virial}} = \frac{\mu m\langle\sigma^2\rangle}{3k} \quad (1.2)$$

where μ is the mean molecular weight, k is the Boltzmann constant, T_{virial} is the virial temperature, m is the mass of a test particle, and $\langle\sigma\rangle$ is the average velocity of the test particle. In this equation, $\langle\sigma\rangle$ can be replaced with the line-of-sight galaxy velocity dispersion (an actual cluster observable) because all objects within the cluster potential (stars, galaxies, protons, kittens, Wall-E, *etc.*) are subject to the same dynamics and hence have comparable thermal and kinetic energies. The virial temperature is a fundamental characteristic of a cluster.

Galaxy clusters are the most massive objects presently in the Universe. The enormous mass means deep gravitational potential wells and hence very high virial temperatures. Most clusters lie in the temperature range $kT_{\text{virial}} = 1 - 15$ keV. At these energy scales gases are collisionally ionized plasmas and will emit X-rays via thermal bremsstrahlung (discussed in Section §1.3.1). The ICM is not a pure ionized hydrogen gas, as a result, atomic line emission from heavy elements with bound electrons will also occur. The ICM is also optically thin at X-ray wavelengths, *e.g.* the ICM optical depth is much smaller than unity, $\tau_{\lambda} \ll 1$, and hence the X-rays emitted from clusters stream freely into the Universe. In the next section I briefly cover the processes which give rise to ICM X-ray emission and the observables which result. For a magnificently detailed treatise of this topic, see Sarazin (1986) and references therein. 

1.3.1 X-RAY EMISSION

Detailed study of clusters proceeds mainly through spatial and spectral analysis of the ICM. By directly measuring the X-ray emission of the ICM, quantities such as temperature, density, and luminosity per unit volume can be inferred. Having this knowledge about the ICM provides an observational tool for indirectly measuring ICM dynamics, composition, and mass. In this way a complete picture of a cluster can be built-up and other processes such BCG star formation, AGN feedback activity,

or using ICM temperature inhomogeneity to probe cluster dynamic state can be investigated. In this section, I briefly cover how X-ray emission is produced in the ICM and how basic physical properties are then measured.


The main mode of interaction in a fully ionized plasma is the scattering of free electrons off heavy ions. During this process, charged particles are accelerated and thus emit radiation. The mechanism is known as 'free-free' emission (ff), or by the tongue-twisting thermal bremsstrahlung (German for "braking radiation"). It is also called bremsstrahlung cooling since the X-ray emission carries away large amounts of energy. The timescale for protons, ions, and electrons to reach equipartition is typically shorter than the age of a cluster, thus the gas particles populating the emitting plasma can be approximated as being at a uniform temperature with a Maxwell-Boltzmann velocity distribution,


$$f(\vec{v}) = 4\pi \left(\frac{m}{2\pi kT} \right)^{3/2} \vec{v}^2 \exp \left[\frac{-m\vec{v}^2}{2kT} \right] \quad (1.3)$$


where m is mass, T is temperature, k is the Boltzmann constant, and velocity, \vec{v} , is defined as $\vec{v} = \sqrt{v_x^2 + v_y^2 + v_z^2}$. The power emitted per cubic centimeter per second ($\text{erg s}^{-1} \text{cm}^{-3}$) from this plasma can be written in the compact form

$$\epsilon^{ff} \equiv 1.4 \times 10^{-27} T^{1/2} n_e n_i Z^2 \bar{g}_B \quad (1.4)$$

where 1.4×10^{-27} is the condensed form of the cgs physical constants and geometric factors associated with integrating over the power per unit area per unit frequency, n_e and n_i are the electron and ion densities, Z is the number of protons of the bending charge, \bar{g}_B is the frequency averaged Gaunt factor (of order unity), and T is the global temperature determined from the spectral cut-off frequency (Rybicki & Lightman, 1986). Below the cut-off frequency, $\nu_c = kT/\hbar$, no photons are created because the energy supplied by charge acceleration is less than the minimum energy

required for creation of a photon. Worth noting is that free-free emission is a two-body process and hence the emission goes as the gas density squared while having a weak dependence on the thermal energy, $\epsilon \propto \rho^2 T^{1/2}$. 

Superimposed on the thermal emission of the plasma are emission lines of heavy element contaminant such as C, Fe, Mg, N, Ne, O, S, and Si. The widths and relative strengths of these spectral lines are used to constrain the metallicity of the ICM, which is typically quantified using units relative to solar abundance, Z_{\odot} . A significant fraction of the  I, $\sim 0.3Z_{\odot}$ (Mushotzky & Loewenstein, 1997; Allen & Fabian, 1998b; Fukazawa et al., 1998), is stellar detritus. In collisionally ionized plasmas with temperatures and metallicities comparable to ICM, the dominant ion species is that of the 'closed-shell' helium-like ground state (K and L-shells) (Peterson & Fabian, 2006). The K and L shell transitions are extremely sensitive to temperature and electron densities, therefore providing an excellent diagnostic for constraining both of these quantities. The strongest K-shell transition of the ICM can be seen from iron at $kT \sim 6.7$ keV. If signal-to-noise of the spectrum is of high enough quality, measuring a shift in the energy of this spectral line can be used to confirm or deduce the approximate redshift, and hence distance, of a cluster. The rich series of iron L-shell transitions occur at $0.2 \lesssim T \lesssim 2.0$ keV and are the best diagnostic for measuring metallicity. For the present generation of X-ray instruments, the L-shell lines are seen as a blend with a peak around ~ 1 keV.

Shown in Figs. 1.4 and 1.5 are the unredshifted synthetic spectral models generated with XSPEC (Arnaud, 1996) of a 2 keV and 8 keV gas. Both spectral models have a component added to mimic absorption by gas in the Milky Way, which is seen as attenuation of flux at $E \lesssim 0.4$  keV. For both spectral models the metal abundance is $0.3 Z_{\odot}$. These two spectral models differ by only a factor of four in temperature but note the extreme sensitivity of both the thermal bremsstrahlung exponential cut-off and emission line strengths to temperature.

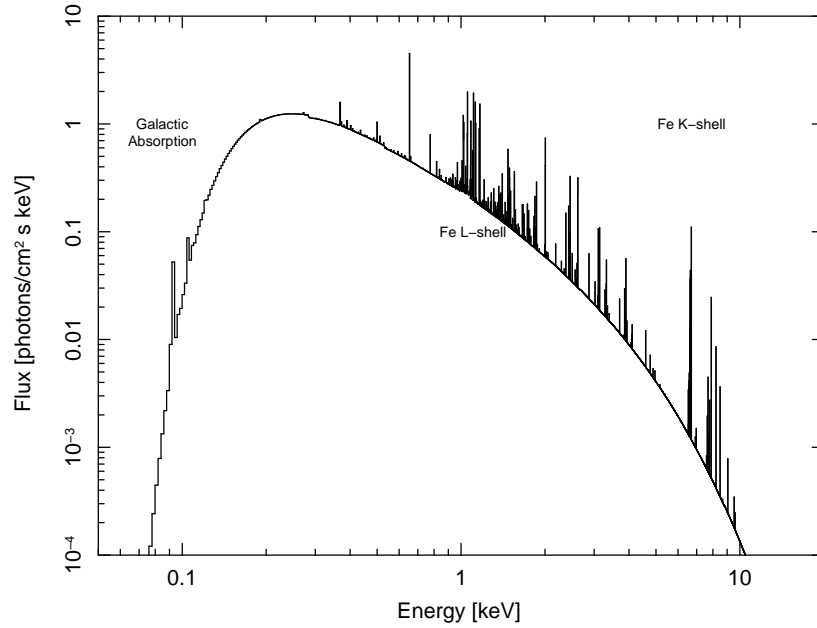


Figure 1.4 Synthetic absorbed thermal spectral model of a $N_H = 10^{20} \text{ cm}^{-2}$, $kT_X = 2.0 \text{ keV}$, $Z/Z_\odot = 0.3$, and zero redshift gas. Notice that the strength of the iron L-shell emission lines is much greater than the iron K-shell lines for this model.

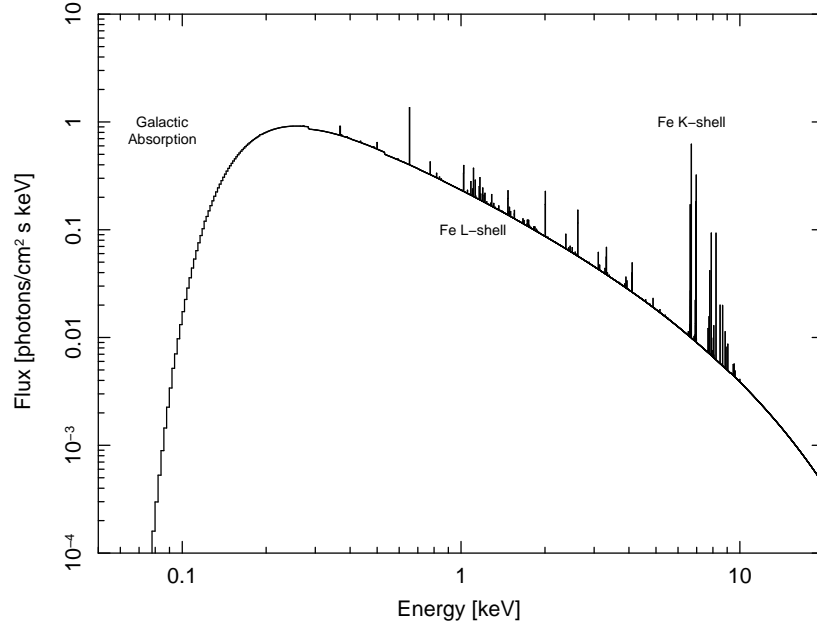


Figure 1.5 Same as Fig. 1.4 except for a $kT_X = 8.0 \text{ keV}$ gas. Notice that for this spectral model the iron L-shell emission lines are much weaker and the iron K-shell lines are much stronger than in the $kT_X = 2.0 \text{ keV}$ model. Also note that the exponential turnover of this model occurs at a higher energy.

Equation 1.4 says that observations of ICM X-ray emission will yield two quantities: temperature and density. The gas density can be inferred from the *emission integral*,

$$EI = \int n_e n_p dV \quad (1.5)$$

where n_e is the electron density, n_p is the density of hydrogen-like ions, and dV is the gas volume within a differential element. The emission integral is essentially the sum of the square of gas density for all the gas parcels in a defined region. Thus, the gas density within a projected volume can be obtained from the spectral analysis, but it can also be obtained from spatial analysis of the cluster emission, for example from cluster surface brightness.

The number of photons detected per unit area (projected on the plane of the sky) per second is given the name *surface brightness*. Assuming spherical symmetry, 2-dimensional surface brightness can be converted to 3-dimensional emission density. By dividing a cluster observation into concentric annuli originating from the cluster center and subtracting off cluster emission at larger radii from emission at smaller radii, the amount of emission from a spherical shell can be reconstructed from the emission in an annular ring. For the spherical shell defined by radii r_i and r_{i+1} , Kriss et al. (1983) shows the relation between the emission density, $C_{i,i+1}$, to the observed surface brightness, $S_{m,m+1}$, of the ring with radii r_m and r_{m+1} , is

$$S_{m,m+1} = \frac{b}{A_{m,m+1}} \sum_{i=1}^m C_{i,i+1} [(V_{i,m+1} - V_{i+1,m+1}) - (V_{i,m} - V_{i+1,m})]. \quad (1.6)$$

where b is the solid angle subtended on the sky by the object, $A_{m,m+1}$ is the area of the ring, and the V terms are the volumes of various shells. This method of reconstructing the cluster emission is called *deprojection*. While assuming spherical symmetry is clearly imperfect, it is not baseless. The purpose of such an assumption is to attain angular averages of the volume density at various radii from an azimuthally

averaged surface density. Systematic uncertainties associated with deprojection are discussed in Section §??.

In this dissertation the spectral model MEKAL (Mewe et al., 1985, 1986; Liedahl et al., 1995) is used for all of the spectral analysis. The MEKAL model normalization, η , is defined as

$$\eta = \frac{10^{-14}}{4\pi D_A^2 (1+z)^2} EI \quad (1.7)$$

where z is cluster redshift, D_A is the angular diameter distance, and EI is the emission integral from eqn. 1.5. Recognizing that the count rate, $f(r)$, per volume is equivalent to the emission density, $C_{i,i+1} = f(r)/\int dV$, where dV can be a shell (deprojected) or the sheath of a round column seen edge-on (projected), combining eqns. 1.6 and 1.7 yields an expression for the electron gas density which is a function of direct observables,

$$n_e(r) = \sqrt{\frac{1.2C(r)\eta(r)4\pi[D_A(1+z)]^2}{f(r)10^{-14}}} \quad (1.8)$$

where 1.2 is the ionization ratio $n_e=1.2n_p$, $C(r)$ is the radial emission density derived from eqn. 1.6, η is the spectral normalization from eqn. 1.7, D_A is the angular diameter distance, z is redshift, and $f(r)$ is the spectroscopic count rate.

Simply by measuring surface brightness and analyzing spectra, the cluster temperature, metallicity, and density can be inferred. These quantities can then be used to derive pressure, $P = nkT$, where $n \approx 2n_e$. The total gas mass can be inferred from $\int(4/3)\pi r^3 n_e$. By further assuming the ICM is in hydrostatic equilibrium, the total cluster mass within radius r is

$$M(r) = \frac{kT(r)}{\mu mG} \left[\frac{d(\log n_e)}{d(\log r)} + \frac{d(\log kT)}{d(\log r)} \right] \quad (1.9)$$

where all variables have their typical definitions. The rate at which the ICM is cooling can also be expressed in simple terms of density and temperature. Given a cooling function, Λ which is sensitive to temperature and metal abundance ($\Lambda(T, Z) \sim 10^{-23}$

for X-ray temperatures), the cooling rate is $r_{cool} = n^2 \Lambda(T, Z)$. For some volume, V , the cooling time is then simply the time required for a gas parcel to radiate away its thermal energy,

$$t_{cool} V r_{cool} = \gamma N k T \quad (1.10)$$

$$t_{cool} = \frac{\gamma n k T}{n^2 \Lambda(T, Z)} \quad (1.11)$$

where γ is a constant specific to the type of cooling process (*e.g.* 3/2 for isochoric and 5/2 for isobaric). The cooling time of the ICM can be anywhere between 10^6 – 10^{10} yrs. Cooling time ~~has historically been~~ a very important descriptor of the ICM because processes such as the formation of stars and line-emitting nebulae are sensitive to cooling time.

By simply pointing an X-ray telescope at a cluster and exposing long enough to attain good signal-to-noise it is possible to derive a host of fundamental cluster properties: temperature, density, pressure, mass, cooling time, and even entropy. Entropy is a very interesting quantity which can be calculated using gas temperature and density and is most likely fundamentally connected to processes like AGN feedback and star formation (discussed in Chapters ?? and 4). In the following section I discuss how gas entropy is derived, why it is a useful quantity for understanding clusters, and how it will be utilized later in this dissertation.

1.3.2 ENTROPY

Entropy has both a macroscopic definition (the measure of available energy) and microscopic definition (the measure of randomness), with each being useful in many areas of science. Study of the ICM is a macro-scale endeavor, so the definition of entropy pertinent to discussion of the ICM is as a measure of the thermodynamic processes involving heat transfer. But the conventional macroscopic definition of

entropy, $dS = dQ/T$, is not that useful in the context of studying astrophysical objects. Thus we must resort to a simpler, measurable surrogate for entropy, like the adiabat. The adiabatic equation of state for an ideal monatomic gas is $P = K\rho^\gamma$ where γ is the ratio of specific heat capacities and has the value of 5/3 for a monatomic gas. Setting $P = \rho kT/\mu m_H$ and solving for K one finds

$$K = \frac{kT}{\mu m_H \rho^{2/3}}. \quad (1.12)$$

where μ is the mean molecular weight of the gas and m_H is the mass of the Hydrogen atom. The true thermodynamic specific entropy using this formulation is $s = k \ln K^{3/2} + s_0$, so neglecting constants and scaling, $s \propto K$ and K shall be called entropy in this dissertation. A further historical simplification can be made to recast eqn. 1.12 using the observables electron density, n_e , and X-ray temperature, T_X (in keV):

$$K = \frac{T_X}{n_e^{2/3}}. \quad (1.13)$$

eqn. 1.13 is the definition of entropy used throughout this dissertation. With a simple functional form, “entropy” can be derived directly from X-ray observations. But why study the ICM in terms of entropy?


ICM temperature and density alone primarily reflect the shape and depth of the cluster dark matter potential (Voit et al., 2002). But it is the specific entropy of a gas parcel, $s = c_v \ln(T/\rho^{\gamma-1})$, which governs the density at a given pressure. In addition, the ICM is convectively stable when $ds/dr \geq 0$, thus, without perturbation, the ICM will convect until the lowest entropy gas is near the core and high entropy gas has buoyantly risen to large radii. ICM entropy can also only be changed by addition or subtraction of heat, thus the entropy of the ICM reflects most of the cluster thermal history⁵. Thus, properties of the ICM can be viewed as a manifestation of the

⁵While the reduction of entropy seems to violate the second law of thermodynamics, recall that ultimately the Universe is the “isolated” system with which clusters interact.

dark matter potential and cluster thermal history - which is encoded in the entropy structure. It is for these reasons that the study of ICM entropy has been the focus of both theoretical and observational study (David et al., 1996; Bower, 1997; Ponman et al., 1999; Lloyd-Davies et al., 2000; Tozzi & Norman, 2001; Voit et al., 2002; Ponman et al., 2003; Piffaretti et al., 2005; Pratt et al., 2006; Donahue et al., 2005, 2006; Morandi & Ettori, 2007; McCarthy et al., 2008).

Radiative cooling and convection of the ICM should result in an entropy distribution which is a power-law across most radii with the only departure occurring at radii smaller than 10% of the virial radius (Voit et al., 2002). Hence deviations away from a power-law entropy profile are indicative of prior heating and cooling and can be exploited to reveal the nature of, for example, AGN feedback. The implication of the intimate connection between entropy and non-gravitational processes being that *both* the breaking of self-similarity and the cooling flow problem can be studied with ICM entropy.

In Chapter ?? and Chapter 4 I present the results of an exhaustive study of galaxy cluster entropy profiles for a sample of 224 galaxy clusters taken from the *Chandra* Data Archive. Analysis of these profiles has yielded important results which can be used to constrain models of cluster feedback, understand truncation of the high-mass end of the galaxy luminosity function, and what affect these processes have on the global properties of clusters. The size and scope of the entropy profile library presented in this dissertation is unprecedented in the current scientific literature, and we hope our library, while having provided immediate results, will have a long-lasting and broad utility for the research community. To this end, we have made all data,

 ~~analysis tools~~, and results available to the public via a project web site⁶.

⁶<http://www.pa.msu.edu/astro/MC2/accept/>

1.4 CHANDRA X-RAY OBSERVATORY

In this section I briefly describe what makes the *Chandra* X-ray Observatory (*Chandra* or CXO for short) a ground-breaking and unique telescope ideally suited for the work carried out in this dissertation. In depth details of the telescope, instruments, and spacecraft can be found at the CXO web sites^{7,8} or in Weisskopf et al. (2000). Much of what is discussed in the following sections can be found with more detail in “The Chandra Proposers’ Observatory Guide.”⁹

1.4.1 TELESCOPE AND INSTRUMENTS

The mean free path of an X-ray photon in a gas with the density of the Earth’s atmosphere is very short. Oxygen and nitrogen in the atmosphere photoelectrically absorb X-ray photons resulting in 100% attenuation and make X-ray astronomy impossible from the Earth’s surface. Many long-standing theories in astrophysics predict a wide variety of astronomical objects as X-ray emitters. Therefore, astronomers and engineers have been sending X-ray telescopes into the upper atmosphere and space for over 30 years now.

The most recent American X-ray mission to fly is the *Chandra* X-ray Observatory. It is one of NASA’s Great Observatories along with *Compton* (γ -rays), *Hubble* (primarily optical), and *Spitzer* (infrared). *Chandra* was built by Northrop-Grumman and is operated by the National Aeronautics and Space Agency. *Chandra* was launched in July 1999 and resides in a highly elliptical orbit with an apogee of $\sim 140,000$ km and a perogee of $\sim 16,000$ km. One orbit takes ≈ 64 hours to complete. The telescope has four nested Iridium-coated paraboloid-hyperboloid mirrors with a focal length of ~ 10 m. An illustration of the *Chandra* spacecraft is shown in Figure 1.6.

⁷<http://chandra.harvard.edu/>

⁸<http://cxc.harvard.edu/>

⁹<http://cxc.harvard.edu/proposer/POG/>

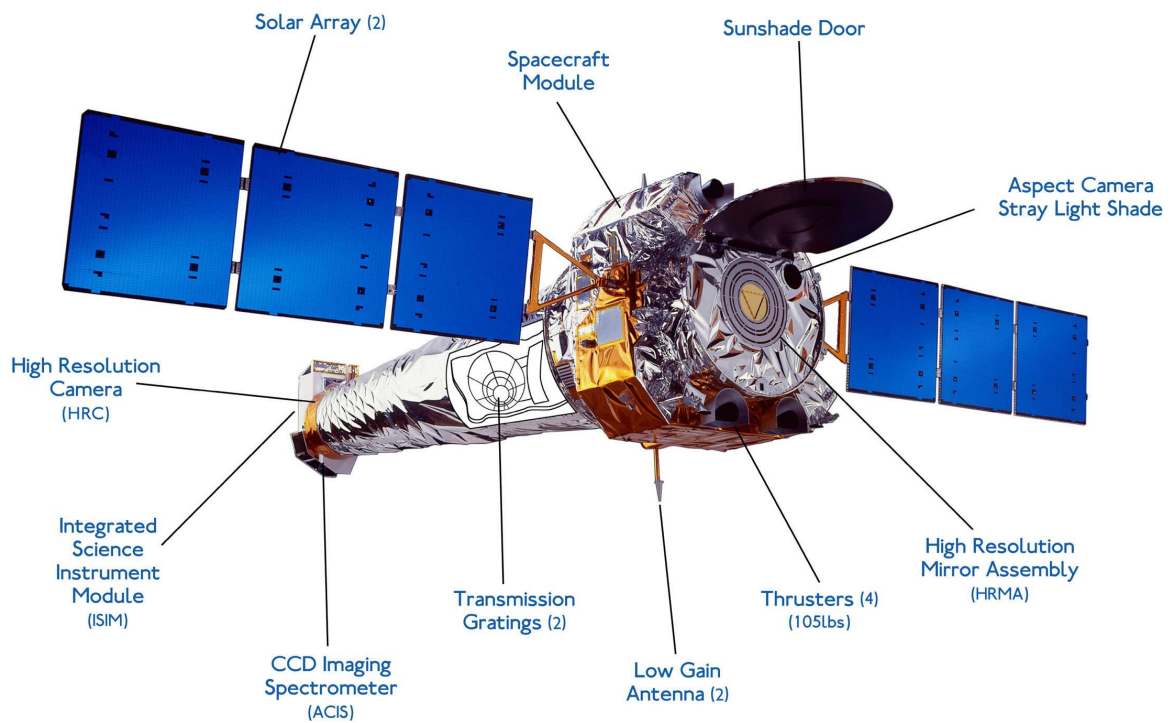


Figure 1.6 An artist's rendition of the *Chandra* spacecraft. *Chandra* is the largest (~ 17 m long; ~ 4 m wide) and most massive (~ 23 K kg) payload ever taken into space by NASA's Space Shuttle Program. The planned lifetime of the mission was 5 years, and the 10 year anniversary party is already planned.

All data presented in this dissertation was collected with the Advanced CCD Imaging Spectrometer (ACIS) instrument¹⁰. ACIS is quite an amazing and unique instrument in that it is an imager and medium-resolution spectrometer at the same time. When an observation is taken with ACIS, the data collected contains spatial and spectral information since the location and energy of incoming photons are recorded. The dual nature of ACIS allows the data to be analyzed by spatially dividing up a cluster image and then extracting spectra for these subregions of the image, a technique which is used heavily in this dissertation.

The observing elements of ACIS are 10 1024×1024 CCDs: six linearly arranged CCDs (ACIS-S array) and four CCDs arranged in a 2×2 mosaic (ACIS-I array). The ACIS focal plane is currently kept at a temperature of ~ -120 °C. A pre-launch photograph of ACIS is shown in Fig. 1.7. During an observation the spacecraft is dithered along a Lissajous curve so parts of the sky which fall in the chip gaps are also observed. Dithering also ensures pixel variations of the CCD response are removed.

The high spatial and energy resolution of *Chandra* and its instruments are ideal for studying clusters of galaxies. The telescope on-board *Chandra* achieves on-axis spatial resolutions of $\lesssim 0.5''/\text{pixel}$ but it is the pixel size of the ACIS instrument ($\sim 0.492''$) which sets the resolution limit for observations. ACIS also has an extraordinary energy resolution of $\Delta E/E \sim 100$. Below energies of ~ 0.3 keV and above energies of ~ 10 keV the ACIS effective area is ostensibly zero. The ACIS effective area also peaks in the energy range $E \sim 0.7 - 2.0$ keV. As shown in Figs. 1.4 and 1.5, a sizeable portion of galaxy cluster emission occurs in the same energy range where the ACIS effective area peaks. The energy resolution of ACIS also allows individual emission line blends to be resolved in cluster spectra. These aspects make *Chandra* a perfect choice for studying clusters and the ICM in detail. Shown in Fig. 1.8 are raw observations of Abell 1795 with the aimpoints on ACIS-I (top panel) and ACIS-S

¹⁰<http://acis.mit.edu/acis>

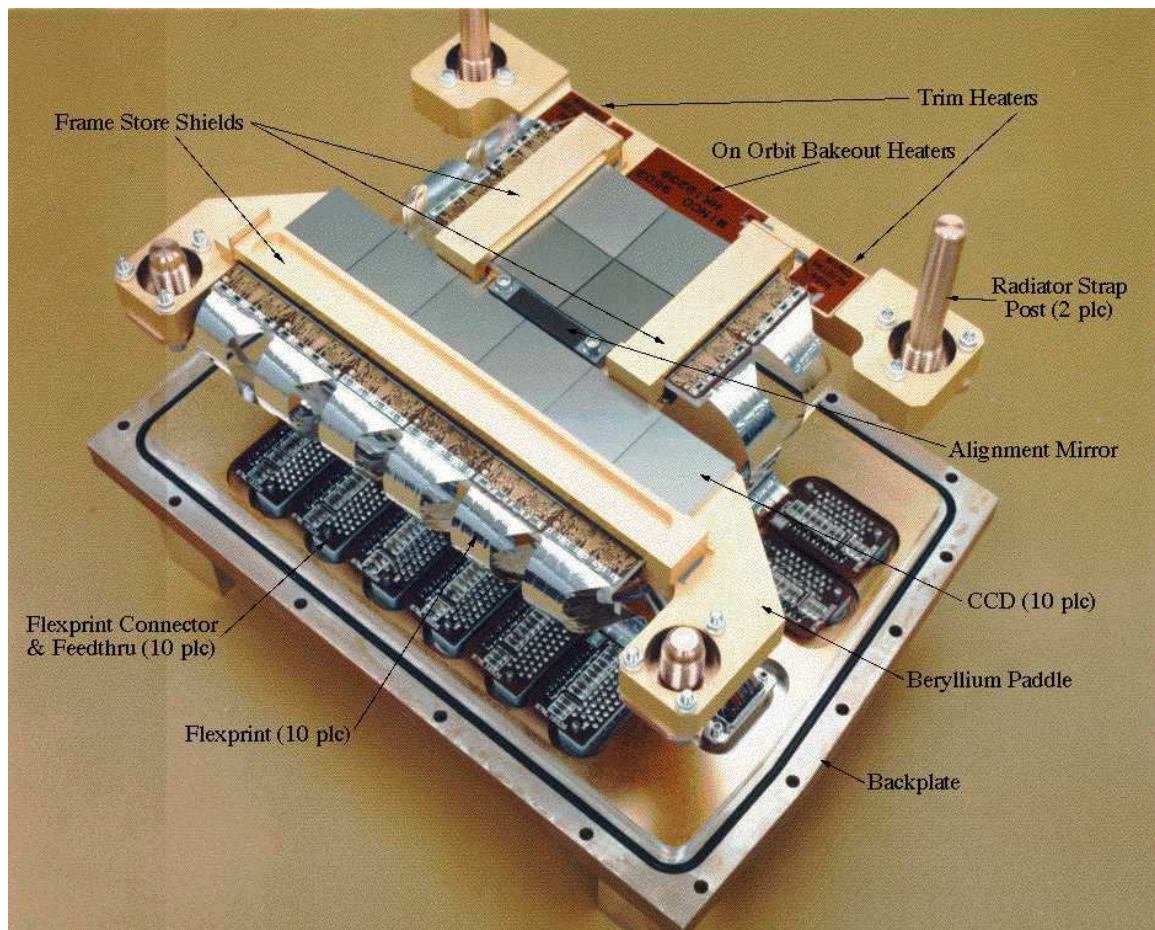



Figure 1.7 This is a pre-launch photograph of the ACIS instrument. The S-array is the line of six CCDs (gray squares) atop the Beryllium Paddle, and the I-array is the mosaic of four CCDs near the On-Orbit Bakeout Heaters. Image taken from Chandra X-ray Center. 

(bottom panel). In Fig. 1.9 is a spectrum for the entire cluster extracted from the ACIS-I observation.

1.4.2 CALIBRATION, BACKGROUND, AND LIFETIME

Chandra is a magnificent piece of engineering, but it is not perfect: observations are contaminated by background, the instruments do not operate at full capacity, and the observatory has a finite lifetime. In this section I briefly discuss these three areas and how they affect past, current, and future scientific study with *Chandra*.

COSMIC X-RAY BACKGROUND (CXB)

Chandra is in a very high Earth orbit and is constantly bathed in high-energy, charged particles originating from the cosmos which interact with the CCDs (the eyes) and the materials housing the instruments (the skull). The CXB is composed of a soft ($E < 2$ keV) component attributable to extragalactic emission, local discrete sources, and spatially varying diffuse Galactic emission. There are also small contributions from the “local bubble” (Snowden, 2004) and charge exchange within the solar system (Wargelin et al., 2004). The possibility of emission from unresolved point sources and other unknown CXB components also exists. In most parts of the sky the soft CXB is not a large contributor to the total background and can be modeled using a combination of power-law and thermal spectral models and then subtracted out of the data.

The CXB also has a hard ($E > 2$ keV) component which arises from mostly extragalactic sources such as quasars and is well modeled as a power-law. The spectral shape of the hard particle background has been quite stable (up until mid-2005) and thus subtracting off the emission by normalizing between observed and expected count rates in a carefully chosen energy band makes removal of the hard component straightforward.

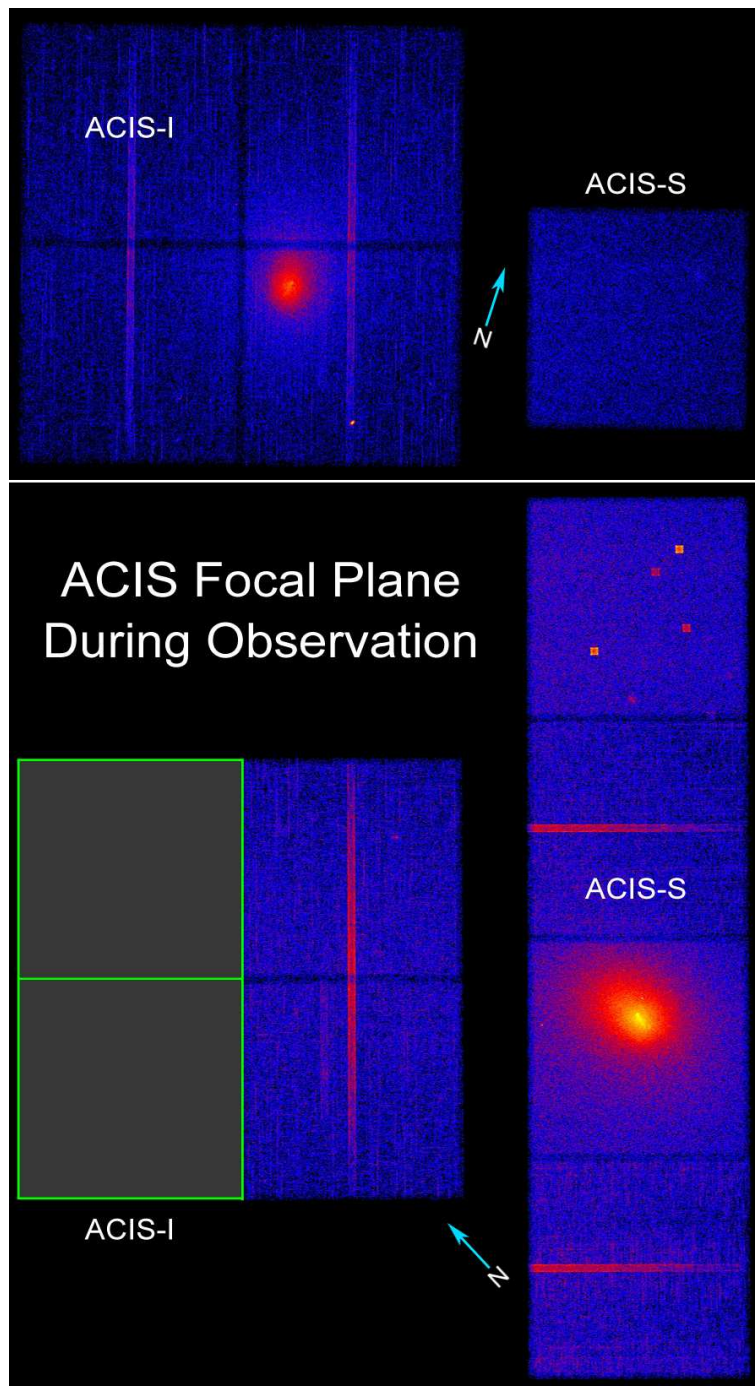


Figure 1.8 In both panels celestial North is indicated by the blue arrow. *Top panel:* ACIS-I aimed observation of Abell 1795. The image has been binned by a factor of four so the whole field could be shown. *Bottom panel:* ACIS-S aimed observation of Abell 1795. Again, the image is binned by a factor of four to show the whole field. For reference, the green boxes mark the ACIS-I chips which were off during this observation.

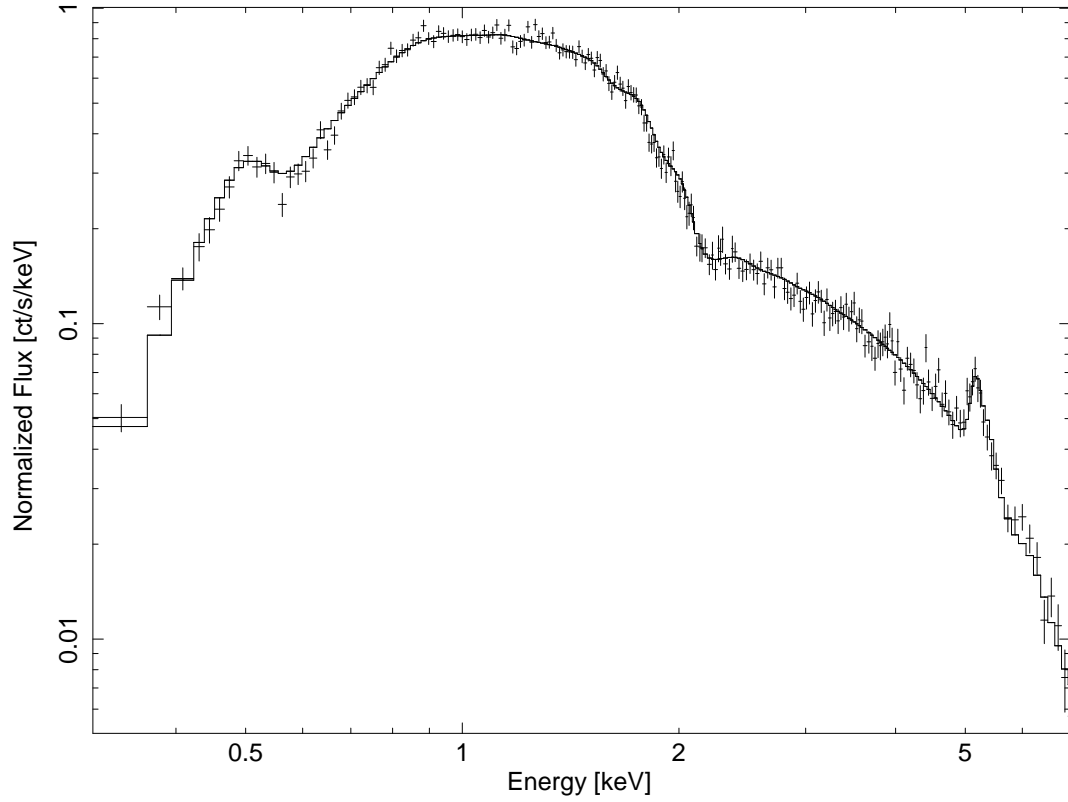


Figure 1.9 Global spectrum of the cluster Abell 1795 with the best-fit single-component absorbed thermal spectral model overplotted (solid line). Comparing this spectrum with those of Figs. 1.4 and 1.5, the effects of finite energy resolution and convolving the spectral model with instrument responses are apparent. Individual spectral lines are now blends, and the spectral shape for $E < 1.0$ keV has changed because of diminishing effective area.

Occasionally there are also very strong X-ray flares. These flares are quite easy to detect in observations because for a judiciously chosen energy band/time bin combination, the count rate as a function of observation time exhibits a dramatic spike during flaring. The time intervals containing flare episodes can be excluded from the analysis rendering the flares harmless to analysis. Harmless that is provided the flare was not too long and some of the observing time allotment is usable.

INSTRUMENTAL EFFECTS AND SOURCES OF UNCERTAINTY

There are a number of instrumental effects which must be considered when analyzing data taken with *Chandra*. The geometric area of the telescope’s mirrors does not represent the “usable” area of the mirrors. The true *effective area* of *Chandra* has been defined by the CXC as the product of mirror geometric area, reflectivity, off-axis vignetting, quantum efficiency of the detectors, energy resolution of the detectors, and grating efficiency (gratings were not in use during any of the observations used in this dissertation). To varying degrees, all of these components depend on energy and a few of them also have a spatial dependence. Discussion of the effective area is a lengthy and involved topic. A more concise understanding of the effective area can be attained from visualization and hence the effective area as a function of energy is shown in Figure 1.10.

The ACIS instrument is also subject to dead/bad pixels, damage done by interaction with very high-energy cosmic rays, imperfect read-out as a function of CCD location, and a hydrocarbon contaminate which has been building up since launch (Marshall et al., 2004).

Observations are also at the mercy of uncertainty sources. The data reduction software provided by the CXC (CIAO) and our own reduction pipeline (CORP, discussed in Appendix ??) takes into consideration:

1. Instrumental effects and calibration

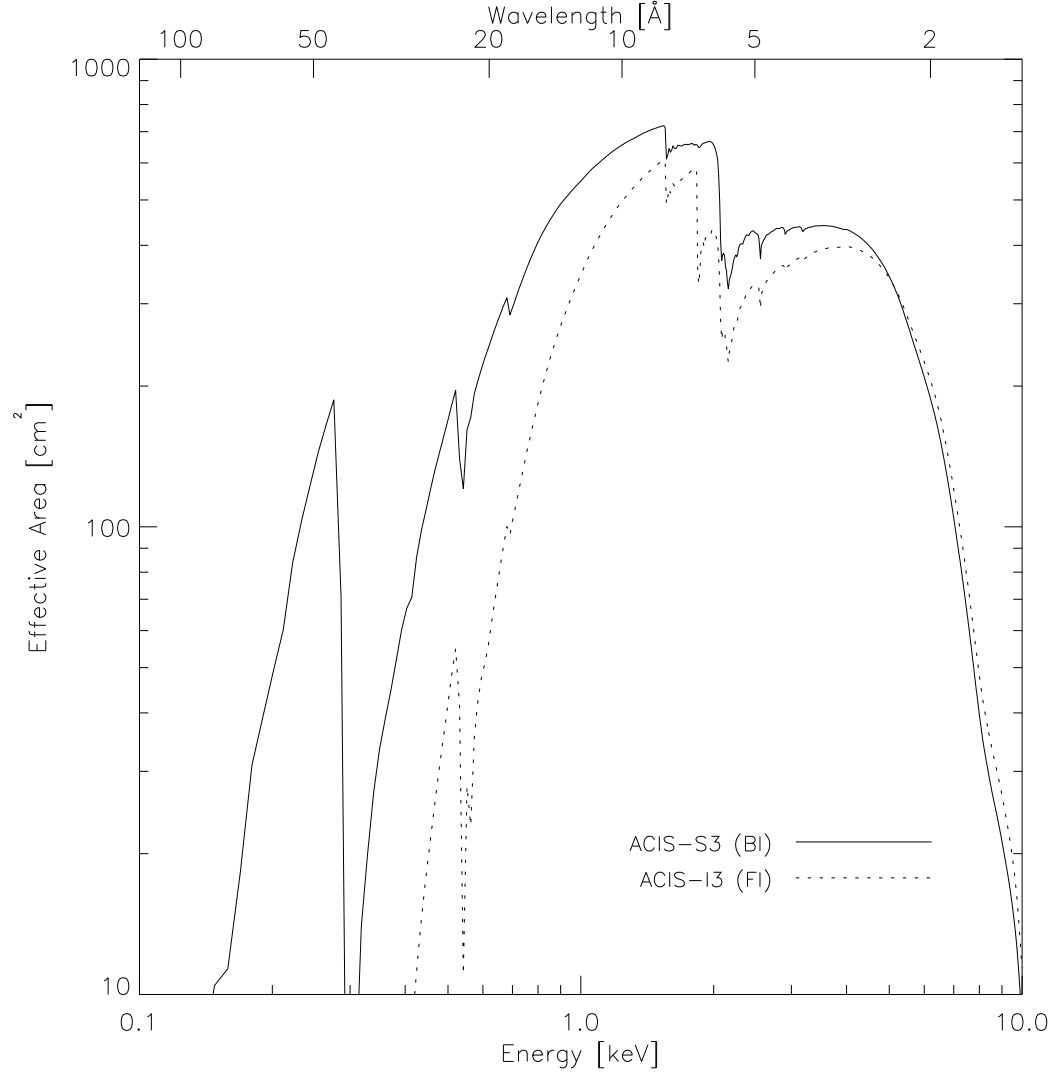



Figure 1.10 *Chandra* effective area as a function of energy. The effective area results from the product of mirror geometric area, reflectivity, off-axis vignetting, quantum efficiency of the detectors, energy resolution of the detectors, and grating efficiency. Note the ACIS peak sensitivity is in the energy range where the majority of ICM occurs, $E = 0.1 - 2.0$ keV.

2. $\approx 3\%$ error in ACIS flux calibration 
3. Statistical errors in the sky and background count rates
4. Errors due to uncertainty in the background normalization
5. Error due to the $\approx 2\%$ systematic uncertainty in the background spectral shape
6. Cosmic variance
7. Unresolved source intensity
8. Scattering of source flux

The list provided above is not comprehensive, but highlights the largest sources of uncertainty: counting statistics, instrument calibration, and background. In each section of this dissertation which discuss data analysis, the uncertainty and error analysis is discussed in the context of the science objectives.




LONG-TERM FUNCTION OF *Chandra*

The *Chandra* mission was scheduled for a minimum five year mission with the expectation that it would go longer. Nearing the ten year anniversary of launch, it is therefore useful to discuss how *Chandra* might be operating in years to come and what the future holds for taking data with *Chandra* five and even ten years from now. The “life expectancy” of *Chandra* can be broken down into the categories spacecraft health, orbit stability, instrument performance, and observation constraint evolution. Much of what is discussed here is given in more detail by Bucher (2007, 2008).

As of *Chandra*’s last review, the health of the spacecraft and its instruments was excellent. The threat from foreseeable major hardware or software failures which would disable or cripple *Chandra*’s science mission is considered to be small. There is the continued accumulation of hydrocarbons on the instruments and possibly mirror, but these problems are known and well modeled. Provided the spacecraft continues

to operate with current capacity and the thermal controls which keep the Sun from baking *Chandra* operate properly, the physical spacecraft and its software should outlive mission funding.

The **non-spherical shape** of the  Sun, Jupiter, Earth, and Moon slowly increase the eccentricity of *Chandra*'s orbit. Consequently there are also changes to the orbit perogee and apogee. At ever decreasing perogee, *Chandra* will spend longer and longer in the Earth's radiation belt, which consequently shortens the avaiable observing time and alters the time allocation schedule. But these effects are predictable and as long as the orbital changes are relatively stable and follow predictions, then the science mission of *Chandra* should not suffer too much.

A less tangible problem is the evolution of observing constraints. In this context constraint means any factor which does not allow the telescope to be in observing mode. Issues which will be addressed as they arise are degradation of the thermal control systems, longer radiation belt transits, complex momentum handling of the spacecraft, smaller area of observation while the telescope is ever closer to Earth, and use of onboard consumables. A less obvious constraint is that as *Chandra* gets older, the number of observable but unobserved objects decreases and the expected number of complex and long observing programs should rise each proposing cycle. How these issues will be resolved is undergoing study.

Given all the factors which can degrade *Chandra*'s science mission, the telescope is expected to complete a 15 year mission (~ 2014). This is good news for X-ray astronomers and the astrophysics community. It is also a testament to the quality of the work by the people that designed, built, launched, and operate the mission.

Chapter Two

Cavagnolo, Kenneth W., Donahue, Megan, Voit, G. Mark, Sun, Ming (2008). Bandpass Dependence of X-ray Temperatures in Galaxy Clusters. The Astrophysical Journal. 0:000-000.

CHAPTER 2:
BANDPASS DEPENDENCE OF X-RAY
TEMPERATURES IN GALAXY
CLUSTERS

Chapter Three

Cavagnolo, Kenneth W., Donahue, Megan, Voit, G. Mark, Sun, Ming (2008). Chandra Archival Sample of Intracluster Entropy Profiles. The Astrophysical Journal Supplement Series. 0:000-000.

CHAPTER 3:
CHANDRA ARCHIVAL SAMPLE OF
INTRACLUSTER ENTROPY
PROFILES

Chapter Four

Cavagnolo, Kenneth W., Donahue, Megan, Voit, G. Mark, Sun, Ming (2008). An Entropy Threshold for Strong $H\alpha$ and Radio Emission in the Cores of Galaxy Clusters. The Astrophysical Journal Letters. 0:000-000.

CHAPTER 4:
AN ENTROPY THRESHOLD FOR
STRONG $H\alpha$ AND RADIO
EMISSION IN THE CORES OF
GALAXY CLUSTERS

CHAPTER 5:

SUMMARY

BIBLIOGRAPHY

REFERENCES

- Alexander, P. 2002, MNRAS, 335, 610
- Allen, S. W., & Fabian, A. C. 1998a, MNRAS, 297, L57
- . 1998b, MNRAS, 297, L63
- Allen, S. W., Fabian, A. C., Johnstone, R. M., White, D. A., Daines, S. J., Edge, A. C., & Stewart, G. C. 1993, MNRAS, 262, 901
- Antonucci, R., & Barvainis, R. 1994, AJ, 107, 448
- Arnaud, K. A. 1996, in ASP Conf. Ser. 101: Astronomical Data Analysis Software and Systems V, ed. G. H. Jacoby & J. Barnes, 17–+
- Arnaud, M., & Evrard, A. E. 1999, MNRAS, 305, 631
- Bauer, F. E., Fabian, A. C., Sanders, J. S., Allen, S. W., & Johnstone, R. M. 2005, MNRAS, 359, 1481
- Bialek, J. J., Evrard, A. E., & Mohr, J. J. 2001, ApJ, 555, 597
- Binney, J., & Tabor, G. 1995, MNRAS, 276, 663
- Blumenthal, G. R., Faber, S. M., Primack, J. R., & Rees, M. J. 1984, Nature, 311, 517
- Borgani, S., Governato, F., Wadsley, J., Menci, N., Tozzi, P., Quinn, T., Stadel, J., & Lake, G. 2002, MNRAS, 336, 409
- Borgani, S., Rosati, P., Tozzi, P., Stanford, S. A., Eisenhardt, P. R., Lidman, C., Holden, B., Della Ceca, R., Norman, C., & Squires, G. 2001, ApJ, 561, 13
- Bower, R. G. 1997, MNRAS, 288, 355
- Bower, R. G., Benson, A. J., Lacey, C. G., Baugh, C. M., Cole, S., & Frenk, C. S. 2001, MNRAS, 325, 497
- Brighenti, F., & Mathews, W. G. 2006, ApJ, 643, 120
- Brüggen, M., & Kaiser, C. R. 2002, Nature, 418, 301
- Brüggen, M., Kaiser, C. R., Churazov, E., & Enßlin, T. A. 2002, MNRAS, 331, 545
- Bryan, G. L., & Norman, M. L. 1998, ApJ, 495, 80
- Bucher, S. 2007, Prospects and Issues for a Fifteen Year Chandra Lifetime

- . 2008, *Chandra News*, 15, 21
- Canizares, C. R., Clark, G. W., Jernigan, J. G., & Markert, T. H. 1982, *ApJ*, 262, 33
- Cavaliere, A., Menci, N., & Tozzi, P. 1999, *MNRAS*, 308, 599
- Churazov, E., Sunyaev, R., Forman, W., & Böhringer, H. 2002, *MNRAS*, 332, 729
- Clowe, D., Bradač, M., Gonzalez, A. H., Markevitch, M., Randall, S. W., Jones, C., & Zaritsky, D. 2006, *ApJ*, 648, L109
- Cowie, L. L., & Binney, J. 1977, *ApJ*, 215, 723
- Dalla Vecchia, C., Bower, R. G., Theuns, T., Balogh, M. L., Mazzotta, P., & Frenk, C. S. 2004, *MNRAS*, 355, 995
- David, L. P., Arnaud, K. A., Forman, W., & Jones, C. 1990, *ApJ*, 356, 32
- David, L. P., Jones, C., & Forman, W. 1996, *ApJ*, 473, 692
- Donahue, M., Horner, D. J., Cavagnolo, K. W., & Voit, G. M. 2006, *ApJ*, 643, 730
- Donahue, M., Mack, J., Voit, G. M., Sparks, W., Elston, R., & Maloney, P. R. 2000, *ApJ*, 545, 670
- Donahue, M., Sun, M., O’Dea, C. P., Voit, G. M., & Cavagnolo, K. W. 2007, *AJ*, 134, 14
- Donahue, M., & Voit, G. M. 2004, in *Clusters of Galaxies: Probes of Cosmological Structure and Galaxy Evolution*, ed. J. S. Mulchaey, A. Dressler, & A. Oemler, 143–+
- Donahue, M., Voit, G. M., O’Dea, C. P., Baum, S. A., & Sparks, W. B. 2005, *ApJ*, 630, L13
- Edge, A. C., & Frayer, D. T. 2003, *ApJ*, 594, L13
- Edge, A. C., & Stewart, G. C. 1991, *MNRAS*, 252, 414
- Edge, A. C., Stewart, G. C., & Fabian, A. C. 1992, *MNRAS*, 258, 177
- Eke, V. R., Navarro, J. F., & Frenk, C. S. 1998, *ApJ*, 503, 569
- Evrard, A. E. 1990, *ApJ*, 363, 349
- Evrard, A. E., & Henry, J. P. 1991, *ApJ*, 383, 95
- Evrard, A. E., Metzler, C. A., & Navarro, J. F. 1996, *ApJ*, 469, 494
- Fabian, A. C. 1994, *ARA&A*, 32, 277

- Fabian, A. C., Allen, S. W., Crawford, C. S., Johnstone, R. M., Morris, R. G., Sanders, J. S., & Schmidt, R. W. 2002, MNRAS, 332, L50
- Fabian, A. C., & Nulsen, P. E. J. 1977, MNRAS, 180, 479
- Fabian, A. C., Nulsen, P. E. J., & Canizares, C. R. 1984, Nature, 310, 733
- Falcke, H., Rieke, M. J., Rieke, G. H., Simpson, C., & Wilson, A. S. 1998, ApJ, 494, L155+
- Finoguenov, A., Reiprich, T. H., & Böhringer, H. 2001, A&A, 368, 749
- Frenk, C. S., White, S. D. M., Bode, P., Bond, J. R., Bryan, G. L., Cen, R., Couchman, H. M. P., Evrard, A. E., Gnedin, N., Jenkins, A., Khokhlov, A. M., Klypin, A., Navarro, J. F., Norman, M. L., Ostriker, J. P., Owen, J. M., Pearce, F. R., Pen, U.-L., Steinmetz, M., Thomas, P. A., Villumsen, J. V., Wadsley, J. W., Warren, M. S., Xu, G., & Yepes, G. 1999, ApJ, 525, 554
- Fukazawa, Y., Makishima, K., Tamura, T., Ezawa, H., Xu, H., Ikebe, Y., Kikuchi, K., & Ohashi, T. 1998, PASJ, 50, 187
- Gursky, H., Kellogg, E., Murray, S., Leong, C., Tananbaum, H., & Giacconi, R. 1971, ApJ, 167, L81+
- Heckman, T. M., Baum, S. A., van Breugel, W. J. M., & McCarthy, P. 1989, ApJ, 338, 48
- Hoeft, M., & Brüggen, M. 2004, ApJ, 617, 896
- Hu, E. M., Cowie, L. L., & Wang, Z. 1985, ApJS, 59, 447
- Jaffe, W., & Bremer, M. N. 1997, MNRAS, 284, L1
- Jeltema, T. E., Hallman, E. J., Burns, J. O., & Motl, P. M. 2007, ArXiv e-prints, 708
- Kaiser, N. 1986, MNRAS, 222, 323
- . 1991, ApJ, 383, 104
- Kriss, G. A., Cioffi, D. F., & Canizares, C. R. 1983, ApJ, 272, 439
- Liedahl, D. A., Osterheld, A. L., & Goldstein, W. H. 1995, ApJ, 438, L115
- Lloyd-Davies, E. J., Ponman, T. J., & Cannon, D. B. 2000, MNRAS, 315, 689
- Loewenstein, M. 2000, ApJ, 532, 17
- Markevitch, M., Forman, W. R., Sarazin, C. L., & Vikhlinin, A. 1998, ApJ, 503, 77
- Markevitch, M., Gonzalez, A. H., David, L., Vikhlinin, A., Murray, S., Forman, W., Jones, C., & Tucker, W. 2002, ApJ, 567, L27

- Markevitch, M., & Vikhlinin, A. 2007, *Phys. Rep.*, 443, 1
- Marshall, H. L., Tennant, A., Grant, C. E., Hitchcock, A. P., O'Dell, S. L., & Plucinsky, P. P. 2004, in Presented at the Society of Photo-Optical Instrumentation Engineers (SPIE) Conference, Vol. 5165, X-Ray and Gamma-Ray Instrumentation for Astronomy XIII. Edited by Flanagan, Kathryn A.; Siegmund, Oswald H. W. Proceedings of the SPIE, Volume 5165, pp. 497-508 (2004)., ed. K. A. Flanagan & O. H. W. Siegmund, 497–508
- Mathews, W. G., & Bregman, J. N. 1978, *ApJ*, 224, 308
- Mathews, W. G., Faltenbacher, A., & Brighenti, F. 2006, *ApJ*, 638, 659
- Mathiesen, B. F., & Evrard, A. E. 2001, *ApJ*, 546, 100
- McCarthy, I. G., Babul, A., Bower, R. G., & Balogh, M. L. 2008, *MNRAS*, 386, 1309
- McCarthy, I. G., Balogh, M. L., Babul, A., Poole, G. B., & Horner, D. J. 2004, *ApJ*, 613, 811
- McDonough, W., & Braungart, M. 2002, *Cradle to Cradle: Remaking the Way We Make Things* (New York: North Point Press)
- McNamara, B. R., & Jaffe, W. 1994, *A&A*, 281, 673
- McNamara, B. R., & Nulsen, P. E. J. 2007, *ARA&A*, 45, 117
- McNamara, B. R., O'Connell, R. W., & Bregman, J. N. 1990, *ApJ*, 360, 20
- Mewe, R., Gronenschild, E. H. B. M., & van den Oord, G. H. J. 1985, *A&AS*, 62, 197
- Mewe, R., Lemen, J. R., & van den Oord, G. H. J. 1986, *A&AS*, 65, 511
- Mitchell, R. J., Culhane, J. L., Davison, P. J. N., & Ives, J. C. 1976, *MNRAS*, 175, 29P
- Mohr, J. J., Mathiesen, B., & Evrard, A. E. 1999, *ApJ*, 517, 627
- Morandi, A., & Ettori, S. 2007, *MNRAS*, 380, 1521
- Mushotzky, R. F. 1984, *Physica Scripta Volume T*, 7, 157
- Mushotzky, R. F., & Loewenstein, M. 1997, *ApJ*, 481, L63+
- Nath, B. B., & Roychowdhury, S. 2002, *MNRAS*, 333, 145
- Navarro, J. F., Frenk, C. S., & White, S. D. M. 1995, *MNRAS*, 275, 720
- . 1997, *ApJ*, 490, 493
- O'Dea, C. P., Baum, S. A., & Gallimore, J. F. 1994a, *ApJ*, 436, 669

- O'Dea, C. P., Baum, S. A., Maloney, P. R., Tacconi, L. J., & Sparks, W. B. 1994b, *ApJ*, 422, 467
- Omma, H., Binney, J., Bryan, G., & Slyz, A. 2004, *MNRAS*, 348, 1105
- Peres, C. B., Fabian, A. C., Edge, A. C., Allen, S. W., Johnstone, R. M., & White, D. A. 1998, *MNRAS*, 298, 416
- Perlmutter, S., Aldering, G., Goldhaber, G., Knop, R. A., Nugent, P., Castro, P. G., Deustua, S., Fabbro, S., Goobar, A., Groom, D. E., Hook, I. M., Kim, A. G., Kim, M. Y., Lee, J. C., Nunes, N. J., Pain, R., Pennypacker, C. R., Quimby, R., Lidman, C., Ellis, R. S., Irwin, M., McMahon, R. G., Ruiz-Lapuente, P., Walton, N., Schaefer, B., Boyle, B. J., Filippenko, A. V., Matheson, T., Fruchter, A. S., Panagia, N., Newberg, H. J. M., Couch, W. J., & The Supernova Cosmology Project. 1999, *ApJ*, 517, 565
- Peterson, J. R., & Fabian, A. C. 2006, *Phys. Rep.*, 427, 1
- Peterson, J. R., Kahn, S. M., Paerels, F. B. S., Kaastra, J. S., Tamura, T., Bleeker, J. A. M., Ferrigno, C., & Jernigan, J. G. 2003, *ApJ*, 590, 207
- Peterson, J. R., Paerels, F. B. S., Kaastra, J. S., Arnaud, M., Reiprich, T. H., Fabian, A. C., Mushotzky, R. F., Jernigan, J. G., & Sakelliou, I. 2001, *A&A*, 365, L104
- Piffaretti, R., Jetzer, P., Kaastra, J. S., & Tamura, T. 2005, *A&A*, 433, 101
- Pizzolato, F., & Soker, N. 2005, *ApJ*, 632, 821
- Ponman, T. J., Cannon, D. B., & Navarro, J. F. 1999, *Nature*, 397, 135
- Ponman, T. J., Sanderson, A. J. R., & Finoguenov, A. 2003, *MNRAS*, 343, 331
- Pratt, G. W., Arnaud, M., & Pointecouteau, E. 2006, *A&A*, 446, 429
- Randall, S. W., Sarazin, C. L., & Ricker, P. M. 2002, *ApJ*, 577, 579
- Riess, A. G., Filippenko, A. V., Challis, P., Clocchiatti, A., Diercks, A., Garnavich, P. M., Gilliland, R. L., Hogan, C. J., Jha, S., Kirshner, R. P., Leibundgut, B., Phillips, M. M., Reiss, D., Schmidt, B. P., Schommer, R. A., Smith, R. C., Spyromilio, J., Stubbs, C., Suntzeff, N. B., & Tonry, J. 1998, *AJ*, 116, 1009
- Riess, A. G., Strolger, L.-G., Casertano, S., Ferguson, H. C., Mobasher, B., Gold, B., Challis, P. J., Filippenko, A. V., Jha, S., Li, W., Tonry, J., Foley, R., Kirshner, R. P., Dickinson, M., MacDonald, E., Eisenstein, D., Livio, M., Younger, J., Xu, C., Dahlén, T., & Stern, D. 2007, *ApJ*, 659, 98
- Roychowdhury, S., Ruszkowski, M., Nath, B. B., & Begelman, M. C. 2004, *ApJ*, 615, 681
- Ruszkowski, M., & Begelman, M. C. 2002, *ApJ*, 581, 223

- Rybicki, G. B., & Lightman, A. P. 1986, *Radiative Processes in Astrophysics* (Radiative Processes in Astrophysics, by George B. Rybicki, Alan P. Lightman, pp. 400. ISBN 0-471-82759-2. Wiley-VCH, June 1986.)
- Sarazin, C. L. 1986, *Reviews of Modern Physics*, 58, 1
- Serlemitsos, P. J., Smith, B. W., Boldt, E. A., Holt, S. S., & Swank, J. H. 1977, *ApJ*, 211, L63
- Sharpee, B., Zhang, Y., Williams, R., Pellegrini, E., Cavagnolo, K., Baldwin, J. A., Phillips, M., & Liu, X.-W. 2007, *ApJ*, 659, 1265
- Snowden, S. L. 2004, in *Astrophysics and Space Science Library*, Vol. 309, *Soft X-ray Emission from Clusters of Galaxies and Related Phenomena*, ed. R. M. J. Lieu, 103–+
- Soker, N., & Pizzolato, F. 2005, *ApJ*, 622, 847
- Spergel, D. N., Bean, R., Doré, O., Nolta, M. R., Bennett, C. L., Dunkley, J., Hinshaw, G., Jarosik, N., Komatsu, E., Page, L., Peiris, H. V., Verde, L., Halpern, M., Hill, R. S., Kogut, A., Limon, M., Meyer, S. S., Odegard, N., Tucker, G. S., Weiland, J. L., Wollack, E., & Wright, E. L. 2007, *ApJS*, 170, 377
- Stewart, G. C., Fabian, A. C., Jones, C., & Forman, W. 1984, *ApJ*, 285, 1
- Tamura, T., Kaastra, J. S., Peterson, J. R., Paerels, F. B. S., Mittaz, J. P. D., Trudolyubov, S. P., Stewart, G., Fabian, A. C., Mushotzky, R. F., Lumb, D. H., & Ikebe, Y. 2001, *A&A*, 365, L87
- Tozzi, P., & Norman, C. 2001, *ApJ*, 546, 63
- Ventimiglia, D. A., Voit, G. M., Donahue, M., & Ameglio, S. 2008, *ArXiv e-prints*, arxiv:0806.0850
- Voit, G. M. 2005, *Reviews of Modern Physics*, 77, 207
- Voit, G. M., & Bryan, G. L. 2001, *Nature*, 414, 425
- Voit, G. M., Bryan, G. L., Balogh, M. L., & Bower, R. G. 2002, *ApJ*, 576, 601
- Voit, G. M., Cavagnolo, K. W., Donahue, M., Rafferty, D. A., McNamara, B. R., & Nulsen, P. E. J. 2008, *ApJ*, 681, L5
- Voit, G. M., & Donahue, M. 1995, *ApJ*, 452, 164
- . 2005, *ApJ*, 634, 955
- Wargelin, B. J., Markevitch, M., Juda, M., Kharchenko, V., Edgar, R., & Dalgarno, A. 2004, *ApJ*, 607, 596

- Weisskopf, M. C., Tananbaum, H. D., Van Speybroeck, L. P., & O'Dell, S. L. 2000, in Presented at the Society of Photo-Optical Instrumentation Engineers (SPIE) Conference, Vol. 4012, Proc. SPIE Vol. 4012, p. 2-16, X-Ray Optics, Instruments, and Missions III, Joachim E. Truemper; Bernd Aschenbach; Eds., ed. J. E. Truemper & B. Aschenbach, 2–16
- White, D. A., Jones, C., & Forman, W. 1997, MNRAS, 292, 419
- White, S. D. M., Efstathiou, G., & Frenk, C. S. 1993, MNRAS, 262, 1023
- White, S. D. M., & Rees, M. J. 1978, MNRAS, 183, 341

APPENDICES

APPENDIX A:

CO-AUTHORED PUBLICATIONS

Listed below are references to publications for which I have contributed work which is not included in this dissertation.

Donahue et al. (2006): The X-ray analysis, entropy profiles, and literature comparison for the nine clusters discussed in this paper were completed by me.

Donahue et al. (2007): I provided some of the analysis for the *Chandra* X-ray data discussed in the paper.

Sharpee et al. (2007): I analyzed the double echelle spectrograph data taken with the MIKE instrument on the Magellan Telescope. The observations were of IC 2501, IC 4191, and NGC 2440.

Voit et al. (2008): The X-ray results presented in this paper were taken from dissertation.